

EFFECT OF HEAT TREATMENT ON MICROSTRUCTURAL AND
MECHANICAL PROPERTIES OF MOLYBDENUM BASED PM FERROUS
ALLOYS

A THESIS SUBMITTED TO
THE GRADUATE SCHOOL OF NATURAL AND APPLIED SCIENCES
OF
THE MIDDLE EAST TECHNICAL UNIVERSITY

BY
RAMONA DAVOUDNEZHAD

IN PARTIAL FULFILLMENT OF THE REQUIREMENTS
FOR
THE DEGREE OF MASTER OF SCIENCE
IN
METALLURGICAL AND MATERIALS ENGINEERING

FEBRUARY 2016

Approval of the thesis:

**EFFECT OF HEAT TREATMENT ON MICROSTRUCTURAL AND
MECHANICAL PROPERTIES OF MOLYBDENUM BASED PM FERROUS
ALLOYS**

submitted by **RAMONA DAVOUDNEZHAD** in partial fulfillment of the requirements for the degree of **Master of Science in Metallurgical and Materials Engineering Department, Middle East Technical University** by,

Prof. Dr. Gülbin Dural Ünver
Dean, Graduate School of **Natural and Applied Sciences**

Prof. Dr. C. Hakan Gür
Head of Department, **Metallurgical and Materials Engineering**

Prof. Dr. Bilgehan Ögel
Supervisor, **Metallurgical and Materials Eng. Dept., METU**

Prof. Dr. Nuri Durlu
Co-Supervisor, **Mechanical Engineering Dept., TOBB ETU**

Examining Committee Members:

Prof. Dr. Rıza Gürbüz
Metallurgical and Materials Engineering Dept., METU

Prof. Dr. Bilgehan Ögel
Metallurgical and Materials Engineering Dept., METU

Prof. Dr. Nuri Durlu
Mechanical Engineering Dept., TOBB ETU

Prof. Dr. C. Hakan Gür
Metallurgical and Materials Engineering Dept., METU

Assoc. Prof. Dr. Y. Eren Kalay
Metallurgical and Materials Engineering Dept., METU

Date: 04/02/2016

I hereby declare that all information in this document has been obtained and presented in accordance with academic rules and ethical conduct. I also declare that, as required by these rules and conduct, I have fully cited and referenced all material and results that are not original to this work.

Name, Last name: Ramona, Davoudnezhad

Signature:

ABSTRACT

EFFECT OF HEAT TREATMENT ON MICROSTRUCTURAL AND MECHANICAL PROPERTIES OF MOLYBDENUM BASED PM FERROUS ALLOYS

Davoudnezhad, Ramona

M. S., Department of Metallurgical and Materials Engineering

Supervisor: Prof. Dr. Bilgehan Ögel

Co-Supervisor: Prof. Dr. Nuri Durlu

February 2016, 85 pages

In this study, the effect of different heat treatment processes on microstructural and mechanical properties of Distaloy-DH and Astaloy Mo (Fe-2Cu-1.5Mo) powders are investigated. Powder samples are sintered at 1120°C for 45 minutes in a sintering furnace under reducing atmosphere of: 10% H₂ + 90% N₂. After sintering, secondary heat treatments are performed on samples. Microstructural characterization of samples is done with optical and electron microscopy. Selective etching is utilized for determining the amount of bainite and martensite in samples. The Distaloy-DH samples yield approximately 1.9% less porosity than Astaloy Mo samples. In all specimens, pearlite, bainite and/or mixture of martensite and bainite phases are obtained based on the isothermal holding temperature or cooling rate from the austenite region. The study revealed that the specimens with martensitic and lower bainitic microstructure yield high TRS values with respect to either pearlitic or upper

bainitic microstructures. Moreover, the lower bainitic structures yield similar or higher TRS values with respect to martensitic structures even at lower hardness values.

Keywords: Powder metallurgy, Isothermal Heat treatment, mechanical properties, bainite morphology

ÖZ

MOLİBDEN ESASLI PM DEMİR ALAŞIMLARINA UYGULANAN ISIL İŞLEMİN İÇYAPI VE MEKANİK ÖZELLİKLERE ETKİSİNİN ARAŞTIRILMASI

Davoudnezhad, Ramona

Yüksek Lisans, Metalurji ve Malzeme Mühendisliği Bölümü

Tez Yöneticisi: Prof. Dr. Bilgehan Ögel

Ortak Tez Yöneticisi: Prof. Dr. Nuri Durlu

Şubat 2016, 85 sayfa

Bu çalışmada, Distaloy-DH ve Astaloy Mo (Fe-2Cu-1.5Mo) tozlarından sinterlenmiş numunelere uygulanan farklı ısıl işlem parametrelerinin içyapı ve mekanik özelliklere olan etkisi araştırılmıştır. Toz numuneler 600 MPa basınç altında preslenmiş ve 1120°C’de sinterleme fırınında 10% H₂ + 90% N₂ ortamında 45 dakika sinterlenmiştir. Numunelere sinterleme işleminden sonra farklı ısıl işlemler uygulanmıştır. Numunelerin içyapı karakterizasyonları optik ve taramalı elektron mikroskopları ile yapılmıştır. Numunelerdeki beynit ve martensit miktarı görüntü analiz yöntemi kullanılarak belirlenmiştir. Yapılan sinterleme sonrası Distaloy DH numunelerinin Astaloy Mo numunelerine göre ortalama %1.9 daha az gözenek içerdiği gözlemlenmiştir. Östenitleme sonrası soğutma hızına veya tuz banyosunda bekletme süresine bağlı olarak numunelerin, martensit, beynit + martensit veya beynit fazına

dönüştüğü görülmüştür. Yapılan çalışmalar, martensitli ve alt beynitli numunelerin, perlitli veya üst beynitli numunelere oranla daha yüksek TRS (Bükme Dayancı) değerleri verdiği görülmüştür. Bunun yanısıra, alt beynitli numunelerin eşit veya daha düşük sertliklerde dahi martensitli numunelerle aynı hatta daha yüksek TRS değerleri verdiği tespit edilmiştir.

Anahtar Kelimeler: Toz metalurjisi, mekanik özellikler, izotermal ısı işlem, beynit morfolojisi

Dedicated to my family for their endless love, support and encouragement

ACKNOWLEDGMENTS

First, I would like to express my sincere gratitude to both of my supervisors Prof. Dr. Bilgehan Ögel and Prof. Dr. Nuri Durlu. I would like to thank Prof. Dr. Bilgehan Ögel for his excellent guidance and for providing the motivation and support that I needed to accomplish this thesis. I would like to thank Prof. Dr. Nuri Durlu for his patience, guidance and support. Thank you so much for believing in my abilities, supporting me, and making this journey such a great experience for me.

I would specially thank to Cengiz Tan and Serkan Yılmaz for their support and help concerning the using of scanning electron microscope and Yusuf Yıldırım for his valuable recommendations and patient help regarding metallographic examinations.

I would like to thank Hakan Hafizoğlu especially for his precious help during the experiments in TOBB ETU.

I am thankful as well to Süha Tirkeş who answered all the questions I had and helped me a lot when I was stuck on a problem.

My greatest gratitude goes to my dear cousin Nima Taheri who patiently revised and corrected my thesis.

My gratitude is also to my lovely cousin Nazli Taheri who made our family happy by her wedding news and increased my motivation during the process of writing the thesis.

I am grateful to my lab mates, Mehmet Dincer, Gülten Kılıç and Güher Tan for their great friendship, brilliant guidance and splendid support during the difficult path of M.S. studies.

I would never forget all the chats and beautiful moments I shared with some of my friends. They were fundamental in supporting me during this stressful and difficult period. I would like to thank Nardin Avishan, Maria Moradnazhad, Nardin Saboonchi, Aras Anari and Touraj Farsadi for their support.

Finally, my deepest gratitude goes to my parents Mahin Hajizadeh and Fereidoun Davoudnezhad and my lovely sister Anahita Davoudnezhad for their unflagging love and unconditional support throughout my life and my studies. They have always strived to provide all the means that were necessary for me to get the best education. I am especially grateful to my mother for her candid comments and fruitful discussions.

TABLE OF CONTENTS

ABSTRACT.....	v
ÖZ.....	vii
ACKNOWLEDGMENTS.....	x
TABLE OF CONTENTS.....	xii
LIST OF TABLES.....	xv
LIST OF FIGURES.....	xvi
CHAPTERS	
1.INTRODUCTION.....	1
2. THEORY AND LITERATURE REVIEW.....	3
2.1 Steps of Powder Metallurgy Process.....	4
2.1.1 Power production-water atomization method.....	5
2.1.2 Alloying Methods in the Preparation of Ferrous Powders.....	6
2.1.2.1 Admixed Ferrous Powders.....	7
2.1.2.2 Prealloyed Ferrous Powders.....	7
2.1.2.3 Partially-Prealloyed (Diffusion Alloyed) Ferrous Powders.....	8
2.1.2.4 Hybrid Ferrous Powders.....	9
2.1.3 Mixing.....	10
2.1.4 Powder compaction.....	10
2.1.5 Sintering of Ferrous Powders.....	10
2.1.6 Supplementary Operations.....	12
2.2 Sinter Hardening.....	13
2.3 General Aspects of Alloying in PM Steels.....	14

2.3.1 The Effect of Alloying Elements on Homogeneity	14
2.3.2 Diffusion of alloying elements	16
2.3.3 The Effect of Alloying Elements on Martensitic and Bainitic Transformation	19
2.3.3.1 Addition of Molybdenum	23
2.3.3.2 Addition of Copper	24
2.3.3.3 Addition of Carbon	25
2.3.4 Iron Based Powders	26
2.3.5 The Aim of the Study	29
3.EXPERIMENTAL PROCEDURE	31
3.1 Powders Used	31
3.2 Experimental Steps	31
3.2.1 Cold Compaction	32
3.2.2 Sintering	33
3.2.3 Heat Treatment Studies	34
3.3 Characterization Studies	35
3.3.1 Optical Microscopy Studies	35
3.3.2 Scanning Electron Microscopy (SEM) Studies	35
3.3.3 Density and Porosity Measurements	35
3.4 Mechanical Characterization	36
3.4.1 Transverse Rupture Strength Tests	36
3.4.2 Macrohardness Tests	36
4.RESULTS	37
4.1 Microstructural Characterization	37
4.1.1 Characterization of As-sintered Specimens	37
4.1.2 Green Density Measurement	39
4.1.3 Porosity Measurement	39
4.2 Characterization of Heat Treated Specimens	41

4.2.1 Microstructural Characterization of Normalized and Quenched Distaloy-DH Specimens.....	42
4.2.2 Microstructural Characterization Isothermally Treated Specimens of Distaloy DH	43
4.2.2.1 Isothermal Treatment of Distaloy DH at 450°C.....	43
4.2.2.2 Isothermal Treatment of Distaloy DH at 300°C.....	46
By deriving M_s value from equation 4.1, isothermal heat treatment on sintered sample at 300°C is done after austenitizing them at 850°C to obtain the morphology of lower bainite in Distaloy-DH. Figure 4.10 shows a general view of Distaloy sample isothermally heat treated at 300°C for 5 minutes. In the same specimen, both martensite and bainite phases are seen. An important point here is that the bainitic reaction is not complete after 5 minutes of isothermal treatment at 300°C.....	46
4.2.3 Microstructural Characterization of Normalized and Quenched Astaloy Mo Specimens	52
4.2.4 Microstructural Characterization Isothermally Treated Specimens of Astaloy Mo.....	54
4.2.4.1 Isothermal Treatment of Astaloy Mo at 450°C	54
4.2.4.2 Isothermal Treatment of Astaloy Mo at 300°C	57
4.3 Hardness Measurements of As-Sintered and Heat Treated Specimens.....	62
4.4 Transverse Rupture Strength Measurements of As-Sintered and Heat Treated Specimens	66
5.DISCUSSION	71
5.1 The Porosity Content of Distaloy DH and Astaloy Mo.....	71
5.2 Microstructural Development of Heat Treated Specimens	72
5.3 Mechanical Characterization of Heat Treated Samples.....	73
6.CONCLUSIONS	77
REFERENCES	81

LIST OF TABLES

TABLES

Table 2.1 Carbon diffusion coefficients in austenitic Fe-Cu-C alloys. (approx. 4wt%C).....	19
Table 2.2 Properties of some Astaloy Mo and Distaloy DH powders compacted under 600 MPa in a lubricated die [13].	27
Table 3.1 The chemical composition of powder mixes.....	31
Table 4.1 Average Density values of compacted and sintered Distaloy-DH and Astaloy Mo powders.....	39
Table 4.2 The amount of porosity of sintered Distaloy DH and Astaloy Mo specimens	39
Table 4.3 Amount of martensite in isothermally treated samples of Distaloy DH at 300°C.....	52
Table 4.4 Amount of martensite in isothermally treated samples of Astaloy Mo at 300°C.....	61
Table 4.5 Summary of phases observed in sintered and austenitized Distaloy DH and Astaloy Mo samples with various heat treatments	62
Table 4.6 Macrohardness values of Distaloy-DH and Astaloy Mo with varying heat treatments	65
Table 4.7 TRS values of Distaloy-DH and Astaloy Mo with varying heat treatments	68

LIST OF FIGURES

FIGURES

Figure 2.1 Application areas of powder metallurgy [1].	3
Figure 2.2 Schematic view of Powder metallurgy process	5
Figure 2.3 (a) water atomization process, (b) powder particle provided by water atomization [10].	6
Figure 2.4: Several alloying methods in the preparation of ferrous powders, (a) hybrid, and (b) prealloyed, (c) partially prealloyed, (d) admixed [11].	7
Figure 2.5: Compressibility curves for fully prealloyed, partially alloyed, and admixed powders (1.8 wt. % Ni, 1.6 wt. % Cu, and 0.55 wt. % Mo) [15].	9
Figure 2.6 Compressibility comparison of prealloying elements when added to iron powder [20].	15
Figure 2.7 Diffusion rates of different alloying elements in Fe expressed as $\log D$ vs $1/T$ [13].	17
Figure 2.8 (a) C and Ni profile in Fe at $t = 0$. (b) C profile after austenitizing. (c) Chemical potential of C vs. distance [29].	18
Figure 2.9 Schematic representation of upper and lower bainite [4].	21
Figure 2.10: Effect of alloying elements on hardenability [32].	22

Figure 2.11 The effect of molybdenum addition in the isothermal transformation diagram of a steel. (a) No molybdenum addition, (b) 0.24% molybdenum addition [33].	23
Figure 2.12 The change of TRS with carbon content at 560 MPa compaction pressure [38].	25
Figure 2.13 The effect of carbon addition in an isothermal transformation diagram of a steel. (a) 0.47% carbon addition, (b) 0.68% carbon addition [33].	26
Figure 2.14 CCT-diagram (top) and amount of phases (bottom) for Distaloy DH-1 + 0,40%C, sintered 30 min at 1120°C in endogas; cooling from 1120°C [13].	28
Figure 2.15 CCT-diagram (top) and amount of phases (bottom) for Astaloy Mo + 0.6%C, sintered 30 min at 1120°C in endogas; cooling from 1120°C [13].	28
Figure 3.1 General view of the compacted sample	32
Figure 3.2: Schematic view of sintering process	33
Figure 3.3 Schematic view of various heat treatments done on samples	34
Figure 4.1 SEM micrograph of Distaloy DH in as-sintered condition. Mainly pearlitic microstructure.....	38
Figure 4.2 SEM micrograph of Astaloy Mo in as-sintered condition. Mainly pearlitic microstructure.....	38
Figure 4.3 Pores are shaded as blue in image analyzer Clemex software. a) Sintered Distaloy-DH, b) sintered Astaloy Mo at a magnification of 100X.	40
Figure 4.4 The microstructure of Distaloy DH after water quenched and tempered. Martensite (M), Porosity (Po).....	42
Figure 4.5 The microstructure of Distaloy-DH after normalizing treatment. The microstructure is a mixture of pearlite (P) and martensite (M).	43

Figure 4.6 SEM micrograph of the Distaloy specimen after an isothermal treatment at 450°C for 5minutes. The microstructure consists of upper bainite	44
Figure 4.7 SEM micrograph of the Distaloy specimen after an isothermal treatment at 450°C for 5minutes. Upper bainite at a higher magnification.....	44
Figure 4.8 SEM micrograph of the Distaloy specimen after an isothermal treatment at 450°C for 30 minutes at a magnification of 900X.....	45
Figure 4.9 SEM micrograph of the Distaloy specimen after an isothermal treatment at 450°C for 30 minutes.....	45
Figure 4.10 SEM micrograph of the Distaloy specimen after an isothermal treatment at 300°C for 5 minutes. Microstructure is a mixture of Lower Bainite and martensite.	46
Figure4.11(a) and (b) SEM micrograph of the Distaloy specimen after an isothermal treatment at 300°C for 5 minutes. Lower Bainite (LB), Martensite (M).	47
Figure 4.12 SEM micrograph of the Distaloy specimen after an isothermal treatment at 300°C for 5 minutes. Lower Bainite(LB),Martensite,.....	48
Figure 4.13 SEM micrograph of the Distaloy specimen after an isothermal treatment at 300°C for 5 minutes with higher magnification	49
Figure 4.14 SEM micrograph of the Distaloy specimen after an isothermal treatment at 300°C for 5 minutes at a magnification of 24,000X with a bainitic morphology	49
Figure 4.15 SEM micrograph of Distaloy Isothermal cooled at 300°C for 30 minutes. Lower bainite at 20000X magnification. Two different morphologies are seen....	50
Figure 4.16 SEM micrograph of Distaloy Isothermal cooled at 300°C for 30 minutes. The bainite sheaves are seen clearly.....	50

Figure 4.17 The change in bainite and martensite content with increasing time of Distaloy.....	51
Figure 4.18 The microstructure of Astaloy Mo after water quenched and tempered. Martensite (M), Porosity (Po). Only martensite phase is seen.	53
Figure 4.19 Pearlite and matrensite phases in Astaloy specimen after a normalizing treatment. Martensite (M), Pearlite (P).....	53
Figure 4.20 The microstructure of Astaloy Mo after normalizing treatment.	54
Figure 4.21 SEM micrograph of the Astaloy specimen after an isothermal treatment at 450°C for 5 minutes with mainly Upper Bainitic morphology.	55
Figure 4.22 SEM micrograph of the Astaloy specimen after an isothermal treatment at 450°C for 30 minutes.....	56
Figure 4.23 SEM micrograph of Astaloy Mo Isothermal cooled at 450°Cfor 30 minutes. At definite regions, the lamellar structure is very fine. fine Lamellar bainite(FB).....	56
Figure 4.24 SEM micrograph of the Astaloy specimen after an isothermal treatment at 300°C for 5 minutes.....	57
Figure 4.25 SEM micrograph of the Astaloy specimen after an isothermal treatment at 300°C for 5 minutes. Martensite (M) and two different morphologies of bainite are observed.....	58
Figure 4.26 SEM micrograph of the Astaloy specimen after an isothermal treatment at 300°C for 30 minutes.....	58
Figure 4.27 SEM micrograph of the Astaloy specimen after an isothermal treatment at 300°C for 30 minutes.....	59

Figure 4.28 SEM micrograph of the Astaloy specimen after an isothermal treatment at 300°C for 30 minutes. Lamellar bainite morphology is seen (12000X magnification).....	59
Figure 4.29 SEM micrograph of the Astaloy specimen after an isothermal treatment at 300°C for 30 minutes. Morphology of lower bainite with high resolution(24,000X).....	60
Figure 4.30 The change in bainite and martensite content of isothermal treated Astaloy at 300°C with increasing time.....	61
Figure 4.31 Macrohardness values of Distaloy DH with varying heat treatments.	63
Figure 4.32 Macrohardness values of Astaloy Mo with varying heat treatments ..	64
Figure 4.33 TRS values of Distaloy DH with varying Heat treatments.	67
Figure 4.34 TRS values of Astaloy Mo with varying Heat treatments.	67
Figure 4.35 Comparison of TRS values for Distaloy and Astaloy of Isothermally heat treated at 300°C with varying times	69
Figure 4.36 Comparison of TRS values for Distaloy and Astaloy of Isothermally heat treated at 450°C with varying times	70
Figure 4.37 Comparison of TRS values for Distaloy and Astaloy with various heat treatments	70

CHAPTER 1

INTRODUCTION

Recently, with the availability of various powder compositions and alloying methods, powder metallurgy has reached a significant place among other methods, used in manufacturing complex parts such as machining, casting, etc. This process includes the mixing, compaction and sintering stages. In order to enhance the product properties such as density, microstructural developments and mechanical properties, secondary operations can be applied [1].

Secondary operations like quenching may cause difficulties. For example, in order to achieve a martensitic microstructure, sintered components must be quenched in oil or water. During the quenching process, oil pierces into pores and it results in the contamination of sintered components [2].

Sinter hardening is a novel process in powder metallurgy that eliminates the necessity of additional secondary heat treatments. In this process, compacts are sintered in an industrial belt furnace, and then sintered parts cooled with different cooling rates flow into the same chamber. Bainite and/or martensite are the main microstructures that are formed after the single step sinter hardening process [3].

A high combination of strength and toughness of bainitic steels attracts attention in recent years. Recently Mo is also used as an important alloying element in bainitic steels [4, 5, 6, 7, 8]. The presence of Mo, together with other alloying elements like Si, Mn, Ni, Cu and B enhances the formation of bainite phase upon continuous cooling and can yield fully bainitic structures. The presence of Mo in Distaloy DH and Astaloy

Mo powders as well as the continuous cooling in sinter hardening may become an important aspect as far as the kinetics of the bainite formation is concerned. However, as far as gathered from the literature, a detailed study on bainitic microstructure of Mo based PM alloys and their effect on mechanical properties are very limited. Also, the behavior of 100% bainitic structures in porous PM components are not well documented.

In this study, the aim is to investigate the formation of bainite and its effect on mechanical properties of sintered Astaloy Mo and Distaloy DH alloys. Distaloy DH is a prealloyed water atomized ferrous powder (Fe-1.5Mo), which is diffusion bonded with 2% Cu. Distaloy DH and Astaloy Mo powders used in the present study have the same composition (Fe-1.5Mo-2Cu). On the other hand, Astaloy Mo is identical to Distaloy DH, but copper is added by the admixing method. After sintering process, the specimens will be heated to austenite region and quenched in salt bath in order to observe the bainite formation characteristics in PM products. It is aimed to obtain not only bainitic, but also bainitic-martensitic microstructures. The effect of microstructure on mechanical properties will be evaluated based on hardness and TRS tests. It is believed that these experiments can generate preliminary data for the sinter hardened PM specimens.

The following chapters include theory and literature review, experimental procedure, results, discussion and conclusions, respectively. In chapter two, important points about sintering and sinter hardening and characterization of different elements and their effects on microstructural and mechanical properties of Fe-C-Cu-Mo system will be explained. In chapter three, the experimental methods of heat treatment of Distaloy DH and Astaloy Mo powders will be described. Chapter four investigates microstructural and mechanical results of the tested specimens. In last chapter, the results will be discussed and compared with related studies in the literature.

CHAPTER 2

THEORY AND LITERATURE REVIEW

Powder metallurgy is one of the most important methods of producing both ferrous and nonferrous metal parts. This study is focused on ferrous powders. A diagram of the applications of powder metallurgy is shown in Figure 2.1 [1].

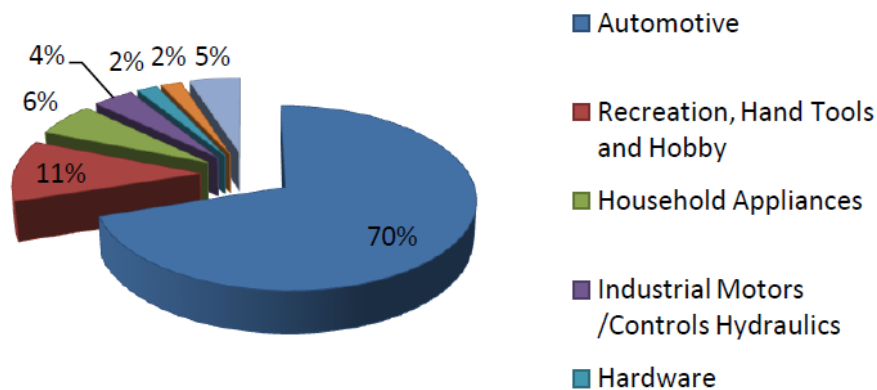


Figure 2.1 Application areas of powder metallurgy [1].

Structural parts contain a huge part of powder metallurgy application. Automotive industry is a big consumer of ferrous powders in structural parts.

Ferrous powder metallurgy in comparison with other production methods like machining, casting and other similar manufacturing ways is an efficient and practical method for production due to the fact that, it is cheaper [1]. Powder metallurgy has several advantages when compared to other manufacturing techniques. By using this

method, manufacturing of complicated shape parts with close tolerances and good dimensional accuracy is attainable. Unlike casting, in this method, all of the raw material is used and therefore no material is being wasted as scrap. The materials can be utilized more conveniently by adopting powder metallurgy than by other methods due to less production difficulties. Therefore, manufacturing some parts such as sintered carbides, self-lubricated bearings and super hard cutting tools is facilitated only with powder metallurgy. Another benefit of this method is that several properties like purity, density, porosity, particle size, etc., can be taken into consideration and carefully controlled during the process. Because of mass-production techniques in powder metallurgy method, high production rates can be easily achieved. Another significant advantage is that highly qualified or skilled labor is not required in the powder metallurgy process [9].

Despite the advantages of powder metallurgy method in producing specific applications, there are some limitations too. Because of high cost of powders, it is not economic to use this method when there is not a mass production. The porosity of products is another problem. The differences between the flow of the powders and the liquid metals cause porosity [9]. In some specific cases, porosity is desirable but in general, it affects the required properties negatively.

2.1 Steps of Powder Metallurgy Process

The main steps of producing PM components are shown in Figure 2.2. This process includes the mixing, compaction and sintering stages. In order to enhance the product properties such as density, microstructural developments and mechanical properties, supplementary operations can be applied. The steps of this process are detailed in the following paragraphs.

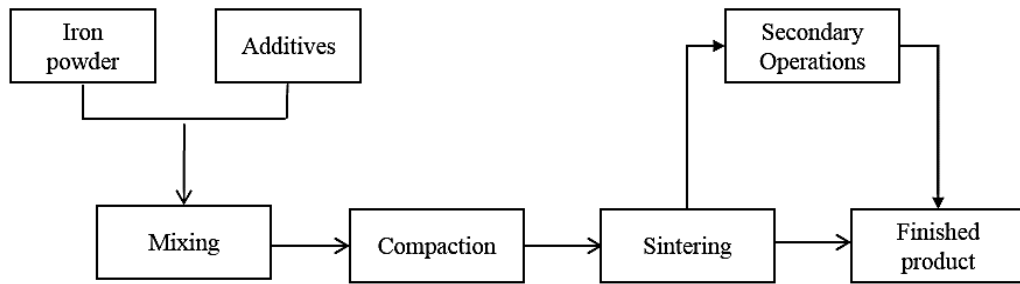


Figure 2.2 Schematic view of Powder metallurgy process

2.1.1 Power production-water atomization method

In the water atomization method, iron scrap and necessary alloying components are chosen as the raw material. The liquid metal flows in a well-controlled stream and is hit by high pressure water jets disintegrating the molten metal stream. Afterwards, the water is directed against the melt stream by a single or multiple jet, or alternatively, employing an annular ring. Owing to the high cooling rate the droplets thus formed solidify precipitously. The particles are irregular, hard and are covered by surface oxides. To diminish surface oxides and consequently to soften the material, the powder is annealed in a reducing atmosphere. One of the salient advantages of the water atomized powders with low impurity levels is being more compressible than the sponge powders. Figure 2.3 demonstrates a sketch of the water atomization technique as well as an example of the process, respectively [10].

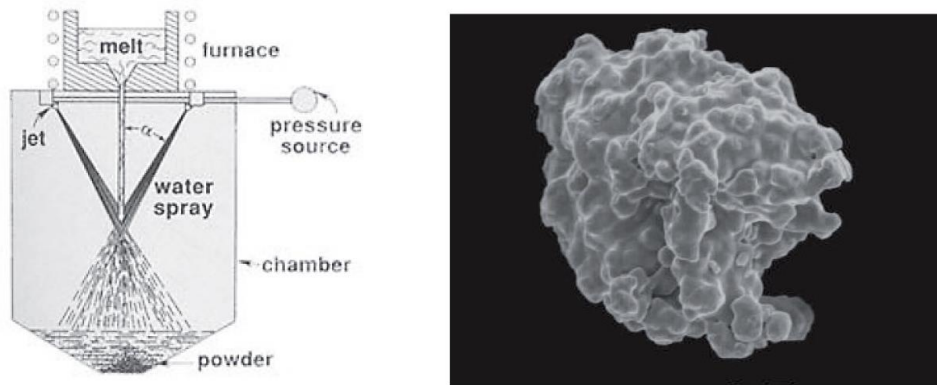


Figure 2.3 (a) water atomization process, (b) powder particle provided by water atomization [10].

2.1.2 Alloying Methods in the Preparation of Ferrous Powders

Alloying and alloying methods have a significant place in powder metallurgy of steels. Each of the various alloying elements used in powder preparing have a different effect on sintering and mechanical properties of the samples. Different types of powders can be used as the starting material for PM steels. Based on the elements used in the mixture and the selected alloying method, microstructure could be homogeneous or heterogeneous. The four different types of powder include admixed, diffusion alloyed, prealloyed and hybrid powders as shown in the Figure 2.4.

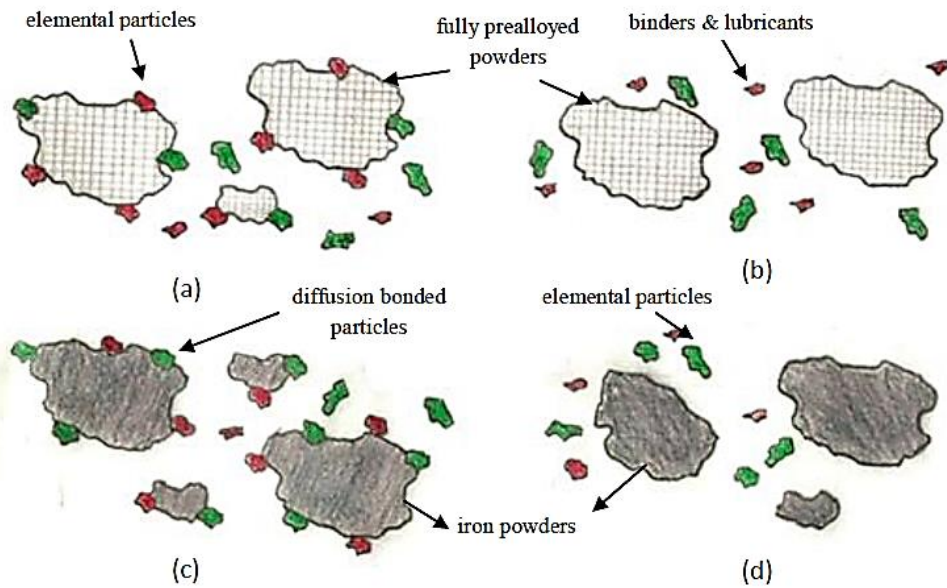


Figure 2.4: Several alloying methods in the preparation of ferrous powders, (a) hybrid, and (b) prealloyed, (c) partially prealloyed, (d) admixed [11].

2.1.2.1 Admixed Ferrous Powders

Admixing is a low-cost method. . In this alloying system, pure iron powders and alloy powders are blended physically; however, there is no chemical mixture in this alloying method. The most common alloying elements are C, Cu, Ni, and Mo. In this single-step method, these alloying elements are mixed with basic powder. Therefore, this method is an easy way to prepare the powder mixture. The powder prepared through this system has a good compressibility but it is not easy to get a uniform mixture [12]. In the sintering step, the temperature is not high enough to give the mixture a chance to diffuse completely [3]. For this reason, admixed powders tolerate a high probability of segregation during handling and assume a heterogeneous microstructure.

2.1.2.2 Prealloyed Ferrous Powders

In the prealloying method, all alloying elements are mixed together and melt. The molten mixture turns into the desired powder by water atomization process. This

method provides a homogeneous and uniform distribution of elements and avoids the problem of segregation. Due to this advantage, there is no need of homogenization during sintering. The compressibility of this method is lower than admixed and diffusion bonded powders [2, 13]. Molybdenum is commonly used in pre-alloyed powders, since it has a relatively small effect on the compressibility [12, 3].

2.1.2.3 Partially-Prealloyed (Diffusion Alloyed) Ferrous Powders

In this method, powders are produced by co-annealing. Ni, Mo and Cu are the common elements used in diffusion-alloyed powders. In this process, alloying elements are mixed with the high purity iron powder (or high compressible prealloyed powder) in a reducing atmosphere. During this process, alloying powder moves to the base powder boundaries and provides inter-particle bonds between alloying elements and base powder. Hence, partially diffused heterogeneous microstructure is obtained. Compressibility of powders are high in this method due to the fact that, the compressibility of base powder is preserved. In addition, there is no segregation problem during handling [14]. James and O'Brien's [12] studies on compaction and sintering behavior of a specific composition provided by admixed, prealloyed, and partially prealloyed methods (1.8 wt. % Ni, 1.6 wt. % Cu, and 0.55 wt. % Mo) shows that prealloyed powder has a higher compressibility compared with elementally admixed and partially prealloyed powders. In this study, a homogenous pearlitic microstructure was observed in case of the prealloyed powder while admixed and partially prealloyed alloys demonstrated a more complex heterogeneous microstructure.

The achievements of Engström et. al. [15] carry out that the compressibility of partially prealloyed and admixed powders is higher than that of prealloyed powders. According to this work, the main reason for this difference is the solid solution strengthening of the alloying elements. In Figure 2.5 the compressibility results of this study are shown.

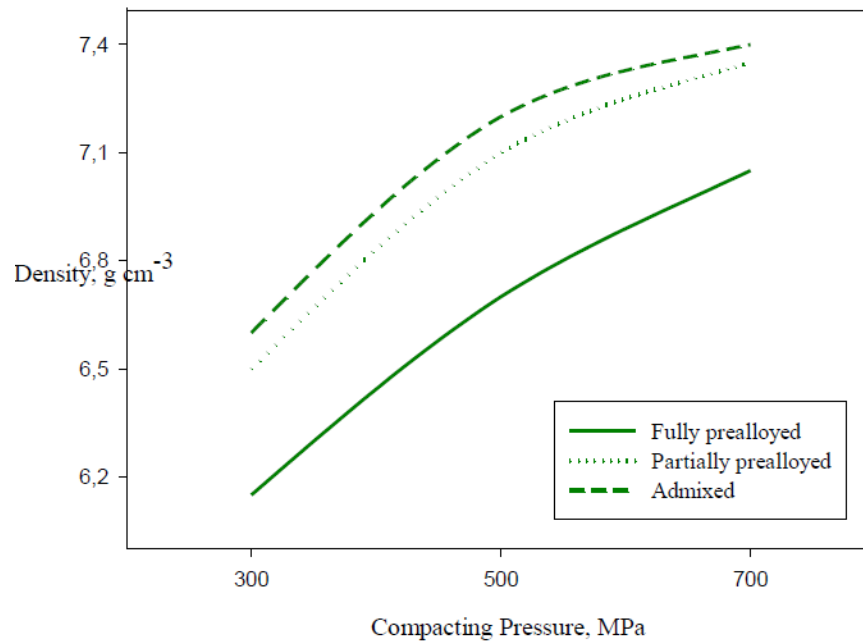


Figure 2.5: Compressibility curves for fully prealloyed, partially alloyed, and admixed powders (1.8 wt. % Ni, 1.6 wt. % Cu, and 0.55 wt. % Mo) [15].

2.1.2.4 Hybrid Ferrous Powders

All the methods introduced above have advantages and disadvantages. Hybrid method is an optimization of these methods according to the final desired properties like hardenability and compressibility. The hardenability of the prealloyed method is higher than the other ones where High compressibility is achieved by admixing or diffusion alloying methods. The hybrid method uses a combination of prealloyed powder with admixed or diffusion alloyed powders [3]. The base powder usually is chosen a prealloyed powder because of its high homogeneity. In sinter hardening, other alloying elements like carbon or copper added by admixing method. The reason is adding these elements by the prealloying method affects strength and compressibility negatively [14].

2.1.3 Mixing

Metal powders, after mixing with binders and lubricants, become ready for pressing in mold under a definite pressure. Lubricants are used to prevent abrasion on mold wall; the binders are added to improve green compact strength.

2.1.4 Powder compaction

In the process of pressing, the powders are compacted with the aid of pressure in a die with an accurate shape and size. The cavity in the die is shaped like the desired product. Metal powders are positioned in the die cavity while the pressing process is carried out with the help of punches pressing the powders from top, bottom, or both [16]. For pressing at low pressure mechanical press machines are preferable whereas hydraulic press machines are the first choice for compacting at high pressure [17]. The pressure applied to the punches has to be delivered in a uniform fashion in order to attain a uniform compressibility of the powders; moreover, it should be high enough to press and establish a mechanical bonding between the powders, a process called cold welding. Subsequent to the compaction, the compacted parts, in the desired shape and size, possess a specific green density and green strength achieved by the cold welding between powder grades; however, the green strength and green density is not high enough for the desired application. These green properties of the material is only useful for handling of the part. To enhance these specific properties and fulfill the necessary requirements, sintering should be done [17].

2.1.5 Sintering of Ferrous Powders

In a typical sintering process, particles are bonded together at high temperatures below the base metal melting point. This metallurgical bonding between particles and neck formation is achieved by decreasing their surface energy.

A sintering furnace conventionally contains a wire mesh to carry the components through its three different zones: the preheat zone, the hot zone, and the cooling zone. In the primary zone, the organic lubricant, i.e. the binder, burns off of the compact. By holding the components in the hot zone, sufficient bonding between the particles can

be attained. Afterwards, parts are cooled down at a definite cooling rate in the cooling zone, depending on the preferred microstructure. The standard sintering temperature for the production of sintered steel parts is 1120°C; the sintering time falls in the range 15-30 minutes. Nevertheless, the optimal condition for most of the alloying systems is not achieved at 1120°C for 15-30 minutes. This obstacle can be averted by employing longer sintering time or higher temperature. High temperature sintering is advantageous for the homogenization of the microstructure due to more rapid diffusion processes, which in some cases can enhance mechanical properties. It also yields a larger number of spherical pores and an improved oxide reduction. High sintering temperature can also result in a number of problems, for instance, shrinkage, decarburization and grain growth [17].

There are three main types of sintering for ferrous powders: solid state sintering, transient liquid state sintering, and activated sintering.

There are two different stages in the sintering process; the early stage with bonding between particles, the late phase of pore rounding, and shrinkage both of which require transport of material. In solid state sintering, various mechanisms of transport are feasible, including volume diffusion, surface diffusion, grain boundary diffusion and evaporation/condensation of atoms on the surface. Liquid phase sintering can be employed to improve the densification process. Throughout the liquid phase sintering, one component of the mixture melts at sintering temperature. The ascending liquid is pulled into pores by way of the capillary forces and creates large contact area between liquid and solid phase, and consequently, enhances the transport rate of material. In activated sintering, a small amount of metal or metal compound, known as activator, is inserted into the base powder. Since the activator has a melting point higher than the sintering temperature, it forms a low melting eutectic together with the base metal substantially accelerating the sintering process [17].

2.1.6 Supplementary Operations

For several applications, sintered components are subjected to supplementary operations, in order to improve properties, obtain final shape and improve appearance. As mentioned earlier, these operations include sizing, infiltration, machining and heat treatment. In this section, only heat treatment is discussed, as it is important in the context of this thesis.

Sintered steel components can be heat treated like conventional steel parts. However, sintered parts may respond somewhat differently than conventional steels, due to their porosity. Heat treatments can be classified as through-hardening, precipitation-hardening and case hardening. In through-hardening, the parts are heated up to the austenitizing temperature and held at that temperature. Then the parts are quenched in oil or water to obtain hard and brittle martensite or bainite. Quenching is followed by tempering to eliminate the high internal stresses. Precipitation hardening is possible in Fe-Cu and Fe-Cu-C alloys due to solubility difference of Cu in austenite and ferrite (9wt% in austenite and 0.4wt% in ferrite). When an iron copper alloy with copper content more than 0.4wt% is heated and cooled rapidly, ferrite supersaturated with copper is formed. Tempering of this supersaturated phase, yields improved hardness and strength due to precipitation of copper particles. Case hardening is a relatively simple and inexpensive way of improving mechanical properties of sintered parts. Among several case hardening techniques carburizing, is briefly discussed here, as the most common one for applications requiring high surface hardness combined with a relatively soft ductile core.

Carbon is added to the surface of the component by heating it in an atmosphere containing methane, butane, carbon monoxide or a combination of gases to provide desired carbon activity. PM components can be heated from 850°C to 920°C for 60 minutes to achieve a certain case depth. The depth of the carbon layer depends on the porosity and the processing time. In sintered parts, carbon penetrates most deeply into parts with the lower density but carburizing is not recommended when the porosity

exceeds 10% due to rapid penetration of carbon and difficult control of carbon potential in the furnace [18].

2.2 Sinter Hardening

In general, the compacted powders require secondary heat treatments to enhance their mechanical properties after the sintering stage. As a result, the secondary heat treatments applied to compacts following sintering can be named as the hardening phase of the powder metallurgy parts. Sinter hardening is a process that combines sintering and hardening stages methodically, within one operation and in the same sintering cycle [19]. Sinter hardening over conventional Q&T (quench and tempering) has a couple of benefits. The main advantage of sinter hardening is its economic nature as a cost reducing process. In industrial operations of powder metallurgy, continuous mesh belt furnaces are employed for sintering to satisfy the urgency for mass production. The sintered parts emerging out of the continuous mesh belt furnace demand secondary heat treatment consisting mainly of oil quenching to enrich the mechanical properties through attaining bainitic and/or martensitic microstructures. The point in the sinter hardening is to facilitate the hardening process by combining sintering and hardening in the same continuous mesh belt furnace. After sintering in the same continuous mesh belt furnace, the hardening phase takes place via gas mixtures and/or air flowing into a separate part of the furnace with a specific flow rate, causing rapid cooling of the sintered parts. The omission of the secondary heat treatments and the prevention of time losses are conducive to cost reduction. The elimination of quench hardening treatment provides a number of alternative critical benefits such as ease of the tempering treatment and a decline in the distortion of the parts. On the other hand, the powder metallurgy products have a porous structure, which poses a big problem owing to the oil contamination of the pores during oil quenching. While sinter hardened parts do not need any additional operation, oil quenched products will certainly require an oil elimination process after quench hardening treatment. Oil contamination also has a negative effect on the tempering treatment, which is mainly applied after the hardening stage to improve the toughness

of the parts. In case of a tempering done at temperatures over 200 °C, the quench hardened parts need to be tempered primarily under 200 °C to clean the oil contamination in the porous structure so that then tempering can be done after this oil removal process. Considering this aspect of the method, tempering for sinter hardened parts is much easier than quench hardened ones. Moreover, quenching also results in surface cracks and dimensional alterations in the parts. Thus, sinter hardening is an appealing technique for a more effective dimensional control due to the distortion lessening in the parts.

2.3 General Aspects of Alloying in PM Steels

This part presents the effect of each alloying element with respect to its contribution to the mechanical and microstructural properties of sintered parts. Those alloying elements that have significant roles in this thesis are taken in to consideration.

2.3.1 The Effect of Alloying Elements on Homogeneity

Adding the alloying elements influences sintering behavior and the compressibility of the powder. Among these elements (Si, Mn and Cr), silicon is the one which affects compressibility more than the others do. The more familiar elements, Mo and Ni, increase the hardness as they dissolve into iron, but the hardening effect of Mo is less than that of Ni. Figure 2.6 shows the effect of various alloying elements on compressibility of the powder [20]. It can be drawn from the Figure 2.6 that for composition like Astaloy Mo (Fe-1.5Mo) compressibility decreases in comparison with pure iron.

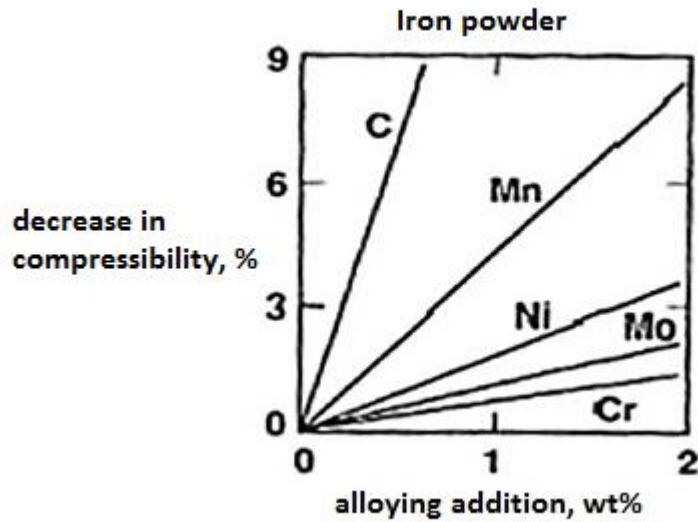


Figure 2.6 Compressibility comparison of prealloying elements when added to iron powder [20].

When carbon is, the only alloying element added to iron at sintering temperatures, a high level of homogeneous distribution is seen in microstructure. Carbon usually added to composition as graphite powder. In case of adding both carbon and copper, it is observed that carbon prohibits copper diffusion homogeneously. Diffusion of carbon in the austenite phase resulted formation of retained austenite at pore surfaces. The amount of retained austenite is not so significant as to affect the performance of the part [14].

Nickel has a smaller diffusion coefficient in austenite as compared to Mo [21] and Cr [22]. So the level of homogeneity of Ni in the composition is lower. For body-centered cubic elements like Cr, Mo, and Si in solid solutions homogenization happens faster. It is observed that diffusivity of elements which forming ferritic alloys are two times more than those forming austenitic solid solutions, like Fe-Ni and Fe-Mn [23].

Studies show that, effect of Cu, Ni, Mo and graphite on mechanical behavior can differ depending on the alloying methods. It was observed that diffusion bonded Mo enhances the tensile strength much more than when Mo is prealloyed or admixed. In

the case of prealloyed Mo, yield strength is better than diffusion bonded one but the tensile strengths and impact energies can compete with each other. As far as the alloying element Cu is concerned, yield strength is not affected so much but tensile strength is improved with smaller size of Cu powder. Coarser copper powder has a negative effect on homogeneity and ductility. In addition, it is observable that the prealloyed Mo material possesses half the level of elongation compared to the case in which diffusion bonding is employed. According to this observation, prealloyed Mo is more sensitive than diffusion bonded Mo to parameters concerning dimensional alteration [27].

2.3.2 Diffusion of alloying elements

This section focuses on the diffusion behavior of each alloying element and the interaction between them. It is assumed that diffusion happens when there is a difference in the concentration of parts. In practice, this is the usual case, but the opposite condition could occur as well. In fact, it is better to define diffusion by the chemical potential gradient so in that case diffusion takes place only to equalize the chemical potential in all regions [28].

In Figure 2.7 the diffusion rate of alloying elements in the iron matrix is shown as a function of $\log D$ versus $1/T$. Nickel, Cu and Mo are substitutional elements so they have a lower diffusion rate in comparison with carbon, which is an interstitial element. Melting point of Cu is lower than that of Ni so Cu can diffuse in the iron matrix faster than Ni. Due to this higher atom mobility, the diffusion rate of Cu in the lattice of iron is much more than that of nickel in a given sintering temperature [13].

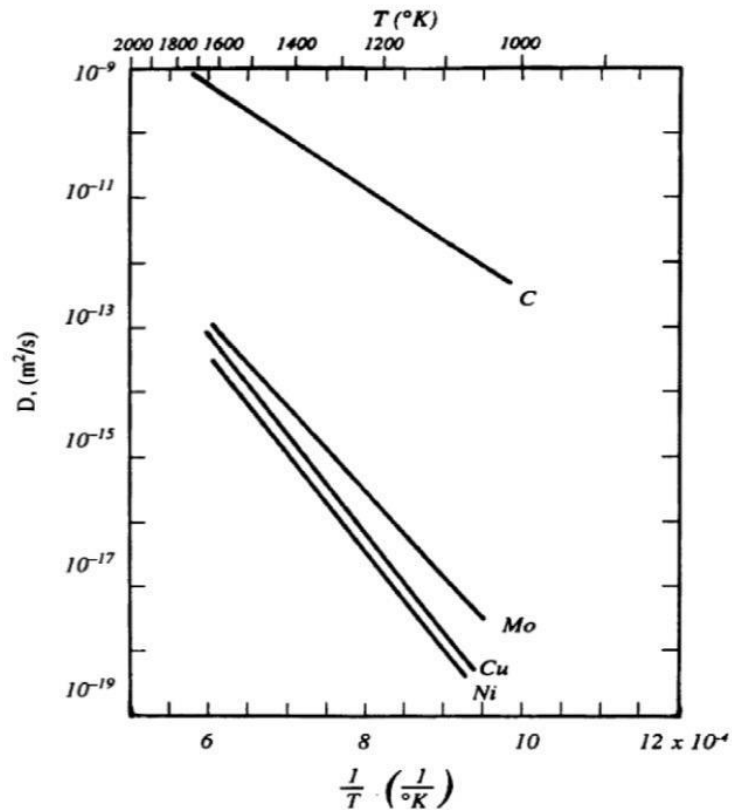


Figure 2.7 Diffusion rates of different alloying elements in Fe expressed as log D vs 1/T [13].

The alloying element with lower melting point diffuses faster. In case of molybdenum, which has a higher melting point compared to other substitutional diffusional elements discussed above, diffusion in iron lattice is faster. This phenomenon can be interpreted by the fact that Mo is a BCC stabilizer whereas Cu and Ni are FCC stabilizers. Diffusion rate in BCC is 100 times more than FCC in a defined temperature [28]. At sintering temperatures, the crystal structure of iron is FCC but when Mo has diffused into FCC lattice, it transforms into BCC. Thus, Mo has a higher diffusion rate compared to Cu and Ni in iron lattice contrary to its higher melting point.

Now the effect of adding a third element to the composition is taken into consideration. Adding another element to the powder can affect the performance of the present

alloying element. In order to get a better view of this concept the Fe-Ni-C system is analyzed. Combining the Ni with Fe-C system resulted in an enhancement in the chemical potential of carbon [29]. In another way, it explains that carbon will diffuse away from Ni-rich regions as well as high carbon concentration places. The profiles of carbon concentration and chemical potential shown below prove this fact. In Figure 2.8.a, there are initial concentration profiles of these pieces of steel, one Fe-Ni-C and the other Fe-C. Fe-C piece has a lower carbon content. For applying a heat treatment these two pieces are attached together. Figure 2.8.b and Figure 2.8.c show carbon concentration and chemical potential results. It can be seen that carbon atoms jump to Ni free side to make the chemical potential equal in both parts. C atoms will be compelled by the diffusion of Ni atoms into Ni free-region to redistribute so as to sustain the chemical potential. Therefore, as long as sufficient amount of time is not granted for the establishment of an equilibrium, a repelling effect between C and Ni will subsist resulting in the non-homogenous distribution of these elements.

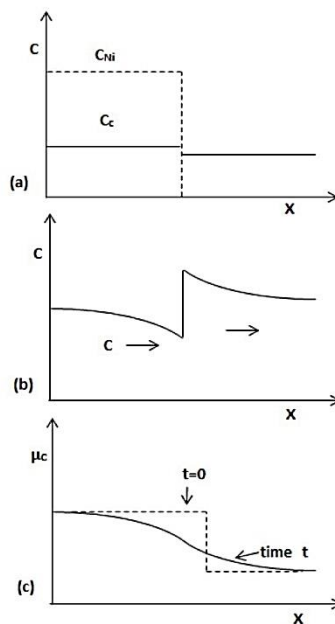


Figure 2.8 (a) C and Ni profile in Fe at $t = 0$. (b) C profile after austenitizing. (c) Chemical potential of C vs. distance [29].

When there is more than one element, the complexity of the diffusional behavior of an element in the iron lattice increases. For example, the diffusion of C in Fe lattice in the presence of Cu, Ni and Mo can be noticed. The purpose of analysis, the distribution of C in the final structure, the weight percent of other elements and the interaction of C with other elements are controlled.

Table 2.1 shows the diffusion coefficient of C in Fe has different Cu contents at 1100°C [26].

Table 2.1 Carbon diffusion coefficients in austenitic Fe-Cu-C alloys. (approx. 4wt% C)

wt% Cu	Diffusion coefficients ($10^{-7} \text{cm}^2/\text{s}$)
1.02	10.1
2.04	11.0
3.10	11.9
3.95	12.6

2.3.3 The Effect of Alloying Elements on Martensitic and Bainitic Transformation

The diffusionless transformation of martensite begins at a temperature named as "Martensite Start", M_s and persists up to a "Martensite Finish" temperature, M_f . The M_s in steels depends on firstly the equilibrium temperature between austenite and ferrite, and secondly the strength of austenite. Both features are altered by the alloying elements, a phenomenon that can be modeled using an empirical relationship formulated by the equation 2.1 [30]

$$M_s (\text{°C}) = 521 - 353C - 225\text{Si} - 24.3\text{Mn} - 27.4\text{Ni} - 17.7\text{Cr} - 25.8\text{Mo} \quad (2.1)$$

The element symbols in the formula refer to their weight percentages. The calculations for steels containing 0.2-0.8% C based on this formula accord well with the data obtained from corresponding experiments. However, for multialloy steels the formula does not at all times provide reliable data for the interaction effects cannot be

designated by a simple summation. Majorly, the dissolved carbon in the austenite affects the M_s values and the M_f declines noticeably as the carbon content increases up to 1% and maintains constancy at higher concentrations of carbon. The determining property of martensitic transformation in steels is that the austenite to martensite transformation is never completely carried out. The transformation begins at the M_s and as the temperature declines up to M_f the amount of martensite increases, and finally at a specific amount of retained austenite is left. In case of the martensite finish temperature being below room temperature, the amount of retained austenite should have an inverse relation to the M_s temperature [11, 19].

The decomposition of the austenite phase at a temperature above M_s but below pearlite formation temperature leads to the formation of bainite phase. Actually, formation of bainite happens in a wide range of temperatures according to various microstructures of this phase. There are two main types of bainite: upper bainite and lower bainite. Upper bainite forms during cooling down from austenite temperature to a range of 500°C to 300°C, and lower bainite temperature range is between 300°C to 200°C, but depends on the amount and type of the alloying elements [31].

It is important to know the upper limit on the isothermal transformation temperature (B_s) to avoid the formation of the pearlite structure. B_s temperature can be estimated using an equation reported in the literature. Equation 2.2 is proposed by Badehshia [4],

$$B_s (\text{°C}) = 830 - 270C - 90Mn - 37Ni - 70Cr - 83Mo \quad (2.2)$$

In which the B_s temperature is defined in centigrade, and the alloying elements are considered in wt %. The average values of B_s temperatures evaluated through these equations were adopted as the upper limit for the isothermal temperatures.

The bainite microstructure includes a non-lamellar mixture of ferrite and carbides. The upper bainite is made up of lath or plate shaped ferrite divided by cementite layers. Lower bainite ferrite consists of needlelike plates or laths with carbides, which precipitated in the lathes (Figure 2.9). These differences in microstructure of two types

of bainite resulted in different mechanical properties. For the same reason, improving the microstructure of low alloy steels directly affects the mechanical properties.

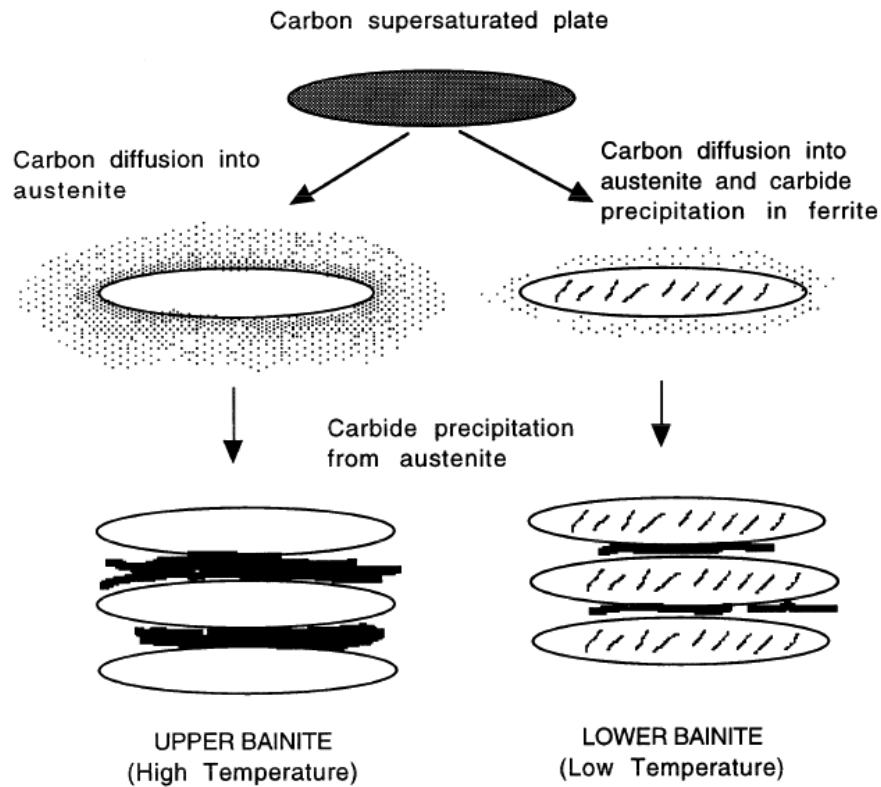


Figure 2.9 Schematic representation of upper and lower bainite [4].

Alloying elements affect a steel in terms of microstructural and thereby mechanical properties. This effect may be observed with isothermal transformation diagrams. In a steel, a change in composition affects the I-T diagrams. The transformation kinetics of austenite to pearlite changes. Increasing the hardenability of steel is the most notable reason for adding alloying elements to powder. Alloying elements delay the time, required for the transformation of austenite to pearlite and ferrite, so the martensitic and bainitic transformations become possible even at slow cooling rates. Figure 2.10 shows the Hardenability factor of various alloying elements. It can be seen from the figure that Mo, Cr and Mn have the most impressive effect on hardenability [32].

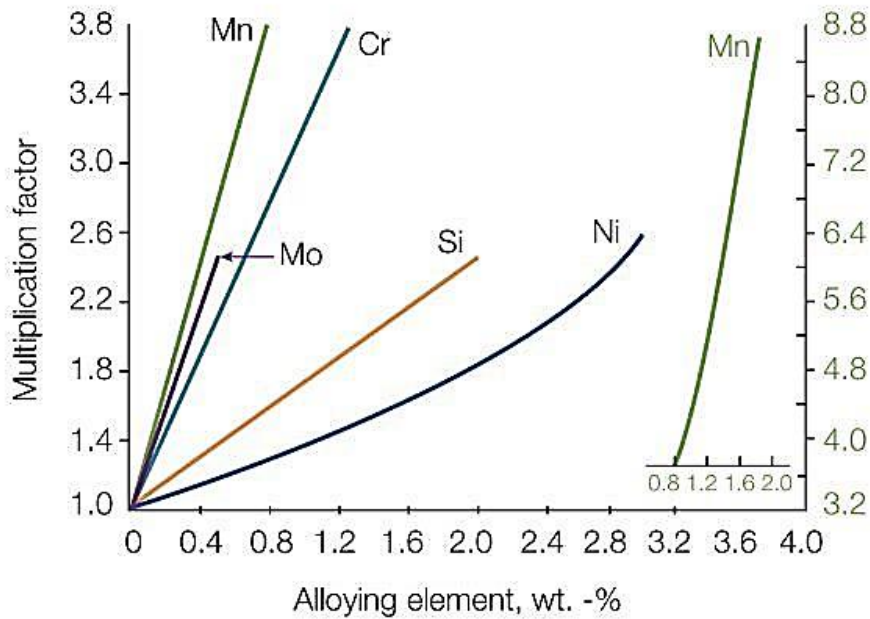


Figure 2.10: Effect of alloying elements on hardenability [32].

The efficiency of alloying elements with respect to their contribution to hardenability decrease in the order of: $Mn > Cr > Mo > Cu > Ni$, Mn being most effective and Ni having the least efficiency. The minimum cooling rate required for the martensite formation depends on the composition of the steel. This, in turn, controls the temperatures and the rates at which the non-martensitic products form and has been studied extensively. The amount of alloying elements and the grain size of austenite can influence the shape and position of curves in TTT and CCT diagrams. However, for nearly all of the alloying elements an increase in their amount can decrease the rate of transformation of austenite to pearlite and austenite to ferrite. They can reduce the nucleation or growth rate of ferrite and pearlite. In fact, the reason for delaying in the transformation is the necessity to wait for the diffusing of alloying elements before nucleation and the growth of the new phase [32].

2.3.3.1 Addition of Molybdenum

As shown in Figure 2.11, adding molybdenum can make changes in the shape of the I-T diagram. The nose of the diagram shift to the right by increasing the amount of Mo from zero to 0.24% wt. This change causes the creation of martensite at slower cooling rates implying an increase in hardenability. Nickel and copper has the same effect as alloying elements [33]. Molybdenum reduces the bainite start temperature, thereby refining the microstructure and leading to the creation of a material with enhanced hardness and strength. Furthermore, the formation of pearlite and ferrite can be suppressed with the aid of Mo, yielding more bainitic microstructure [34] [35].

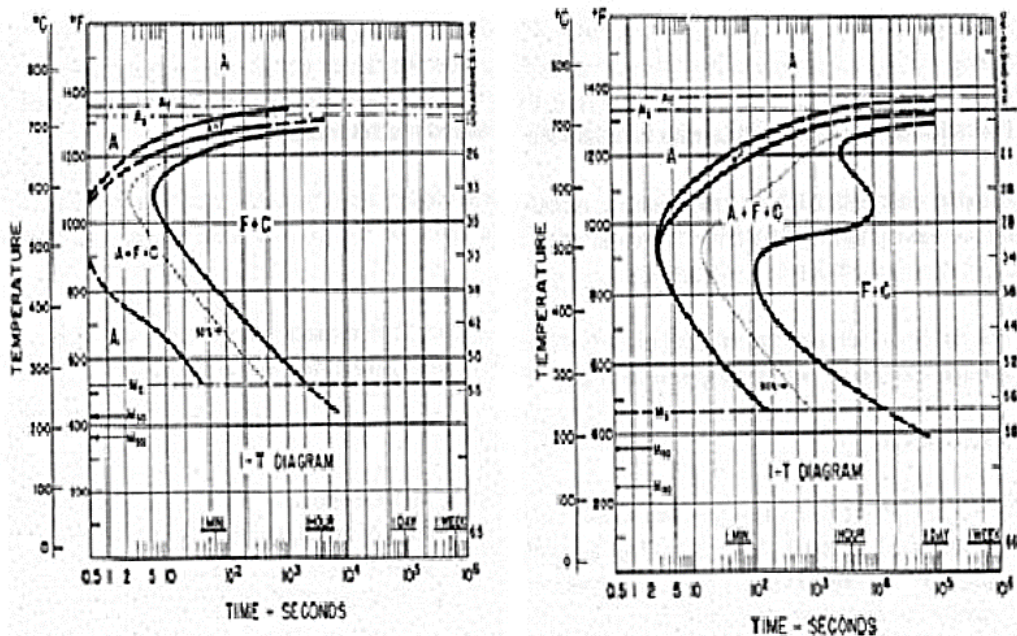


Figure 2.11 The effect of molybdenum addition in the isothermal transformation diagram of a steel. (a) No molybdenum addition, (b) 0.24% molybdenum addition [33].

The price of Mo is increasing because it is one of the significant alloying elements in sinter hardening. This element is commonly used as prealloyed powder because of its homogeneous distribution in the microstructure. Although Mo causes a small decrease

in compressibility but it is regarded as negligible, since its solid solution hardening effect on the iron is considerably low [35, 36].

The results of Causron's [35] experiments demonstrated that increasing the amount of prealloyed Mo enhances the hardenability and in fact the amount of martensite phase in sinter-hardening materials.

Adding molybdenum as an admixed powder showed heterogeneous distribution because of its slow rate of diffusion into base powder [29].

2.3.3.2 Addition of Copper

Adding copper to the base powder can be done by different methods, because the melting point of copper is below the sintering temperature. In admixing method, both C and Cu are added to the system and an enhancement in hardenability is observed. Carbon diffuses into base powder initially and throughout the sintering Cu becomes liquid [14]. By increasing the amount of carbon, diffusion of copper becomes more difficult. As a result, copper starts diffusing into the particles and grain boundaries. These local diffusion leads to a decrease in the temperature of the final martensite. This local change causes retained austenite formation along the grain boundaries. It can be prohibited by lowering the cooling rate. Decreasing the cooling rate leads to the creation of intermediate phases like ferrite and carbide instead of the retained austenite [37].

Using the prealloyed copper prevents the liquid phase sintering of copper. When copper is prealloyed with molten steel through the water atomization, solid state sintering becomes the dominating mechanism. Therefore, there is not any liquid copper around the grain boundaries.

Moreover, copper's effect on mechanical properties was suggested by Baran [38]. He inferred that, when added 1%, copper enhances mechanical features. Beyond this amount, there is no further contribution (Figure 2.12).

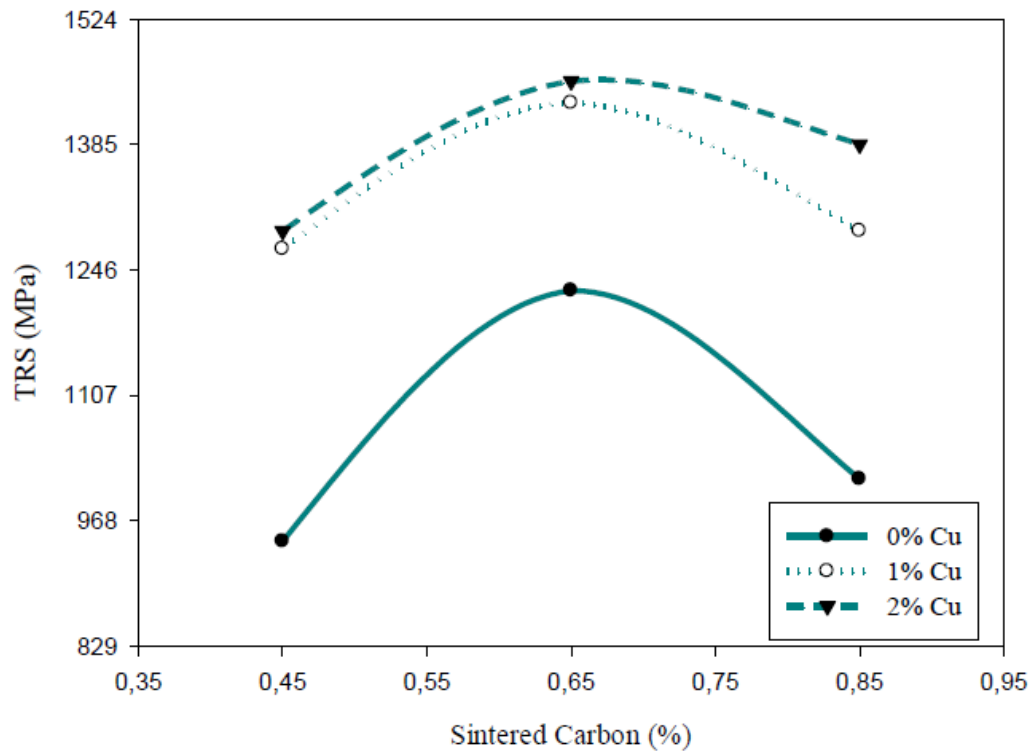


Figure 2.12 The change of TRS with carbon content at 560 MPa compaction pressure [38].

2.3.3.3 Addition of Carbon

In sinter hardening process, typically, carbon is added to base powder as graphite by the admixing method [39, 40, 41]. The quantity of the added graphite is of utmost importance. Increasing the amount of graphite results in the enhancement of the TRS values up to 0.8% C [41, 38]. This is the consequence of martensitic transformation. They concluded that in sinter hardening, an apparently insignificant change of the carbon content could result in a considerable variation in case of the prealloyed [38]. Beyond 0.8%, the TRS values diminish owing to the brittleness brought about by the presence of grain boundary carbides [41, 38]. This decline in the TRS values can also be attributed to the decrease in M_s temperatures as the amount of graphite is increased. The variations of TRS with carbon content is shown in Figure 2.12.

Distaloy DH contains 2%Cu and 1,5%Mo, and is produced by diffusion-bonding 2%Cu-powder to Astaloy Mo. Admixed with graphite, this material can be transformed into a very hard martensitic-bainitic microstructure directly from sintering heat, when the belt furnace is equipped with a convective cooling system allowing cooling rates of 4 - 8°C/s. With these cooling rates, tensile strength values up to 1100 N/mm² are achievable. Properties of Astaloy Mo and Distaloy DH powders are presented below [13].

Table 2.2 Properties of some Astaloy Mo and Distaloy DH powders compacted under 600 MPa in a lubricated die [13].

Powder grade	Particle size (µm)	Apparent density (g/cm ³)	C%	Green density (g/cm ³)	Green strength (MPa)
Astaloy Mo	20 – 180	3.28	0.01	7.14	22
Distaloy-DH	20 – 180	3.41	0.01	7.13	29

By mixing Astaloy and Distaloy powders with suitable amounts of graphite, high strength, good dimensional stability during sintering, and a very well response to subsequent heat-treatment is obtained. Here are two examples of hardenability and microstructural properties of these materials on CCT diagrams.

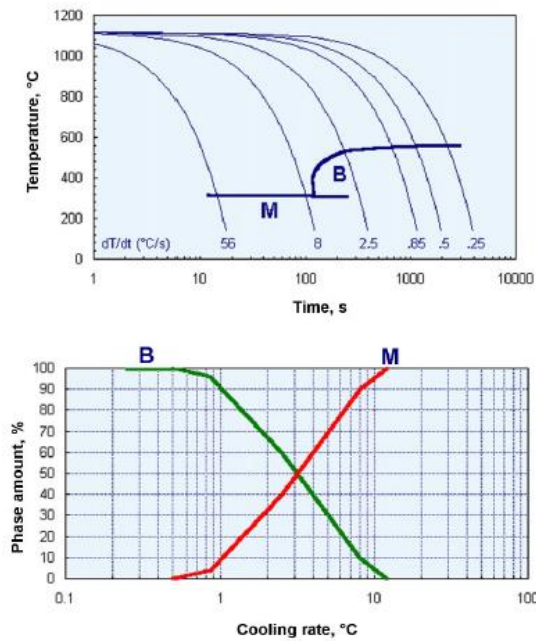


Figure 2.14 CCT-diagram (top) and amount of phases (bottom) for Distaloy DH-1 + 0,40%C, sintered 30 min at 1120°C in endogas; cooling from 1120°C [13].

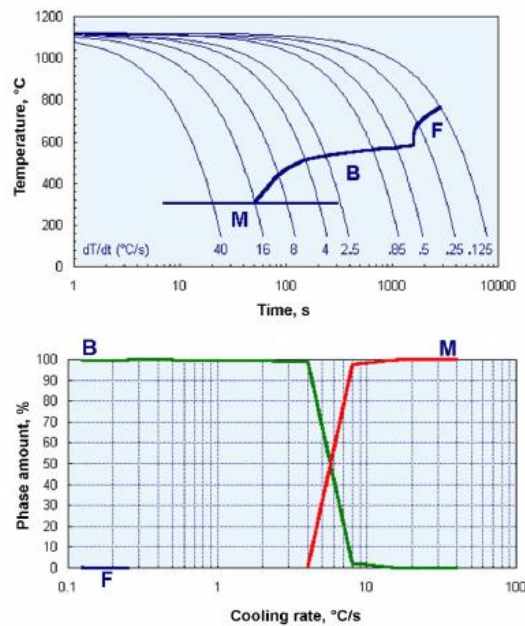


Figure 2.15 CCT-diagram (top) and amount of phases (bottom) for Astaloy Mo + 0.6%C, sintered 30 min at 1120°C in endogas; cooling from 1120°C [13].

2.3.5 The Aim of the Study

Distaloy DH powder contains 1.5% molybdenum, which is added to improve the hardenability and mechanical properties as discussed in the previous sections. This improvement can be attributed to an increase in the amount of martensite due to enhanced hardenability. However, recently Mo is also used as an important alloying element in bainitic steels [4, 5, 6, 7, 8]. The presence of Mo, together with other alloying elements like Si, Mn, Ni, Cu and B enhances the formation of bainite phase upon continuous cooling and can yield fully bainitic structures. A high combination of strength and toughness of bainitic steels attracts attention in recent years. The presence of Mo in Distaloy-DH powder as well as the continuous cooling in sinter-hardening may become an important aspect as far as the kinetics of the bainite formation is concerned. However, as far as gathered from the literature, a detailed microstructural study of bainitic transformations in Mo and Cu containing PM alloys are not studied. Also, the behaviour of 100% bainitic structures in porous PM components are not well documented.

In this study, the aim is to obtain fully bainitic and bainite martensite mixtures in sintered Astaloy Mo and Distloy DH specimens. The salt bath will be used to quench specimens from austenitization temperature to bainite transformation temperatures.

CHAPTER 3

EXPERIMENTAL PROCEDURE

3.1 Powders Used

In the present study, Distaloy-DH and Astaloy Mo powders are used. Distaloy-DH is a trademark of prealloyed powders developed by Hoeganaes. Both of them are prealloyed powders. On the other hand, Astaloy Mo is identical to Distaloy-DH, but copper is added by admixing method. The carbon compositions of both powders are adjusted by admixing. The size of the powder particles is in 20 μ m- 180 μ m range where the average particle sizes are 50 μ m to 60 μ m. These powders were produced by Hoeganaes water atomizing process. The studied compositions of powder alloys are given in Table 3.1.

Table 3.1 The chemical composition of powder mixes

Base powder	C (%)	Cu (%)	Mo (%)	Fe (%)
Distaloy-DH	0.7	2	1,5	Bal.
Astaloy Mo	0.7	2	1,5	Bal.

3.2 Experimental Steps

This study included several steps. At the first step of experiment, the powder mixtures are pressed into the desired shape. Then, the prepared samples were sintered and

austenitized. The final step was the secondary processes. In these processes, various heat treatments were applied.

3.2.1 Cold Compaction

Distaloy-DH and Astaloy Mo powders were compacted at 600 MPa using Instron tension-compression testing machine in a single end die press. The compaction mechanism was unidirectional. The velocity of the compression was 1 mm/min. The dimensions of rectangular compacts were 6 mm in height, 12.8 mm in width, and 31.8 mm in length. These compacts were prepared according to TS 4222 EN ISO 3325 standards for three point bending tests. The weight of specimens were approximately 17 gr for Distaloy powder and 18gr Astaloy powder. The densities of the specimens after compaction were measured approximately 6.95 gr/cm³ for Distaloy samples and 6.87 gr/cm³ for Astaloy samples. Figure 3.1 shows a compacted sample.



Figure 3.1 General view of the compacted sample

3.2.2 Sintering

These compacts were sintered in the laboratory scale furnace. In sintering process, Green samples were preheated up to 600°C. Then, samples were kept at that temperature for 30 minutes in order to remove the binding additives and lubricants from green compacts as a prerequisite for sintering. After removing the binders, specimens were heated to 1120°C at a rate of 10 degrees per minute and held at this temperature for 45 minutes. After sintering was completed, the furnace was cooled to room temperature at a cooling rate of 7 degree per minute reached to 25°C under reducing atmosphere of: 10% H₂+90% N₂. The schematic sintering cycle is given in Figure 3.2.

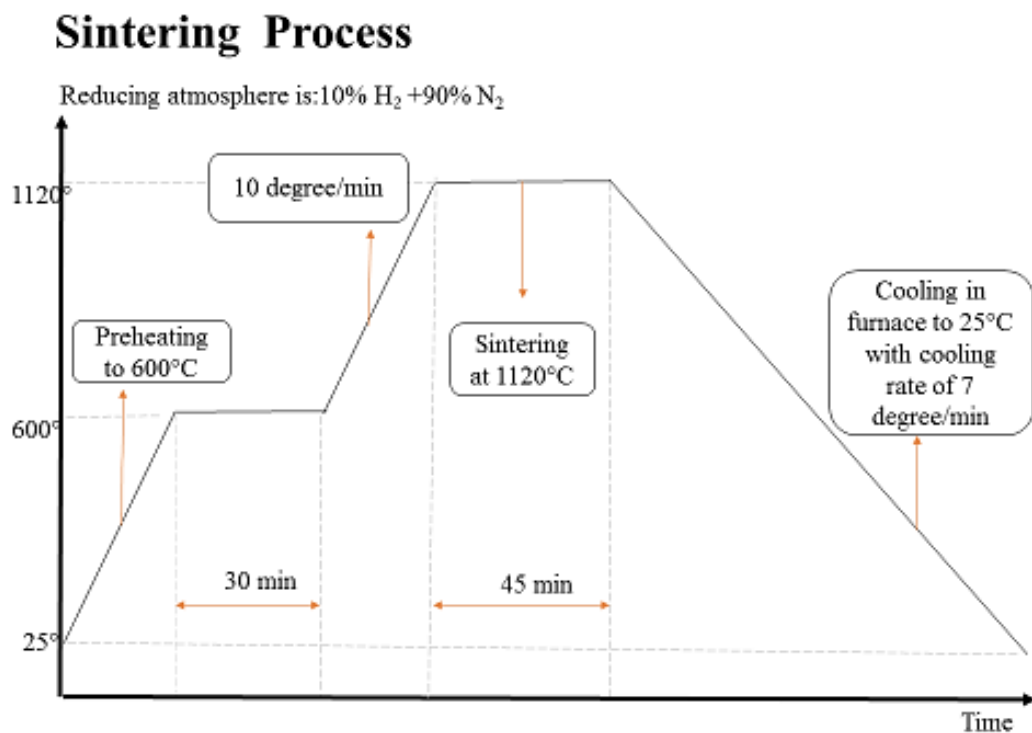


Figure 3.2: Schematic view of sintering process

3.2.3 Heat Treatment Studies

Secondary heat treatment was done on samples after sintering. In secondary heat treatment, samples were austenitized at 850°C for 30 minutes. Before austenizing, samples were covered with copper foil having a thickness of 10 micron in order to protect them from decarburization. The austenitized samples were quenched into salt bath at either 450°C or 300°C for 5minutes, 15minutes, and 30 minutes. After the isothermal treatment in the salt bath was finished, all the samples were water quenched. Several other samples were either water quenched or air-cooled to room temperature without isothermal treatment. A schematic view of applied heat treatments is shown in Figure 3.3.

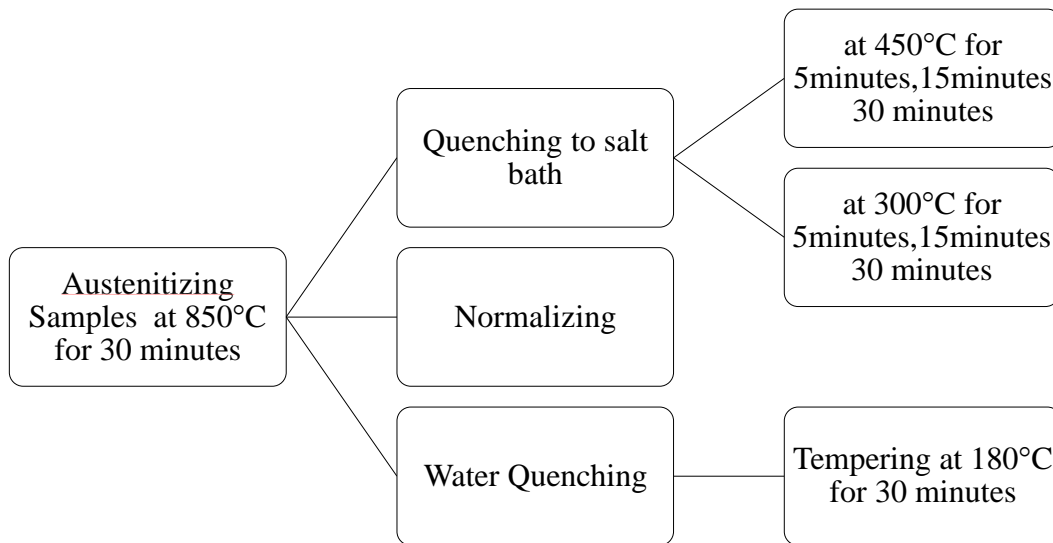


Figure 3.3 Schematic view of various heat treatments done on samples

3.3 Characterization Studies

The characterization of samples included different stages; a) coding samples, b) metallography preparation, c) optical microscopy, d) scanning electron microscopy, e) density and porosity measurements and f) mechanical tests.

3.3.1 Optical Microscopy Studies

For metallographic examination, samples were cut from one-half of the transverse rupture test (TRS) samples. The samples were mounted into Bakelite in order to make the sample preparation easier. Mounted samples were grinded by Metkon Gripo 2V Grinder (Turkey). The samples were polished by Mecapol P230 Polisher (France) (6 μ m diamond) and Metaserv Universal Polisher, England (3 μ m diamond). Preparation of specimens was challenging because of their porous structure. Porosity is harmful for the etching step. Polishing lubricant, alcohol, or diamond particles can be left in porosities despite cleaning the surface of the specimen. During etching, they can come out from porosities and the microscopic image of samples will be clear. In order to remove the foreign particles from the porosity, samples were kept in ethanol for 24 hours and then the samples were cleaned by ultrasonic cleaner for 10 minutes. The etchant was 2% Nital solution. In order to determine the phases in the microstructure, different etching times were used in this study. The optical micrographs were taken with optical microscope Huvitz HDS-5800, Korea.

3.3.2 Scanning Electron Microscopy (SEM) Studies

SEM was used to investigate the morphologies of the powders and phases. Jeol (JSM 6400, Jeol LTD, Tokyo, Japan) and SEM (Nova Nano SEM 430, FEI LTD, Oregon, USA) equipped with EDX analyzer system were used for the examination.

3.3.3 Density and Porosity Measurements

The amount of porosity in the samples were measured with quantitative metallography. Clemex (Vision Professional Edition image analysis system version 3.5.020) was used

for quantitative metallography. The density of the compacted samples was calculated by measuring the dimensions and weighting the samples.

3.4 Mechanical Characterization

3.4.1 Transverse Rupture Strength Tests

The transverse rupture strengths (TRS) test was performed by Instron testing machine (5 tons capacity). The specimens were broken using the three-point bending test set-up under transverse loading. These tests were done according to TS 4222 EN ISO 3325 standards. The velocity of the compression was 1 mm/min. and the dimensions of the compacts were 31.8 x12.8 x6 mm. After measurements, the values of transverse rupture strength were calculated using the formula

$$\text{TRS} = \frac{3PL}{t^2w} \quad (3.1)$$

where, TRS is Transverse rupture strength in N/mm², P is the fracturing (rupture) load (N), L is the distance between the supporting rods, t is the thickness of the sample in (mm) and W is the width of the sample in (mm).

3.4.2 Macrohardness Tests

Macrohardness measurements were done to determine the hardness of the whole structure including porous regions. Macrohardness measurements were taken on Brinell scale using a Wilson-Wolpert hardness machine. Brinell microhardness measurement were done under 187.5 kg load and the used ball size diameter is 2.5 mm. For each sample measuring repeats four times.

CHAPTER 4

RESULTS

4.1 Microstructural Characterization

4.1.1 Characterization of As-sintered Specimens

In this study, the microstructures of Distaloy DH and Astaloy Mo samples are examined after various heat treatment processes. Figure 4.1 and Figure 4.2 show the microstructure of sintered Distaloy DH and Astaloy Mo respectively. In both alloys, the sintered microstructure is pearlitic. The morphology of the pearlite, however, is different from the classical lamellar microstructure of pearlite in plain carbon steels. This is probably due to the presence of alloying elements Mo and Cu, which affects pearlite formation.

In Distaloy DH, Cu is diffusion bonded to prealloyed Fe-1.5Mo alloy powder. Hence, Cu is in solid solution and as a result of this during sintering of samples lower porosity is formed. On the other hand, in Astaloy Mo, Cu is added to the prealloyed Fe-1.5Mo powder alloy. Hence, during sintering Cu melts and penetrates to Fe grain boundaries and this leads to highly porous microstructure. This point will be discussed in the following section on density measurements.

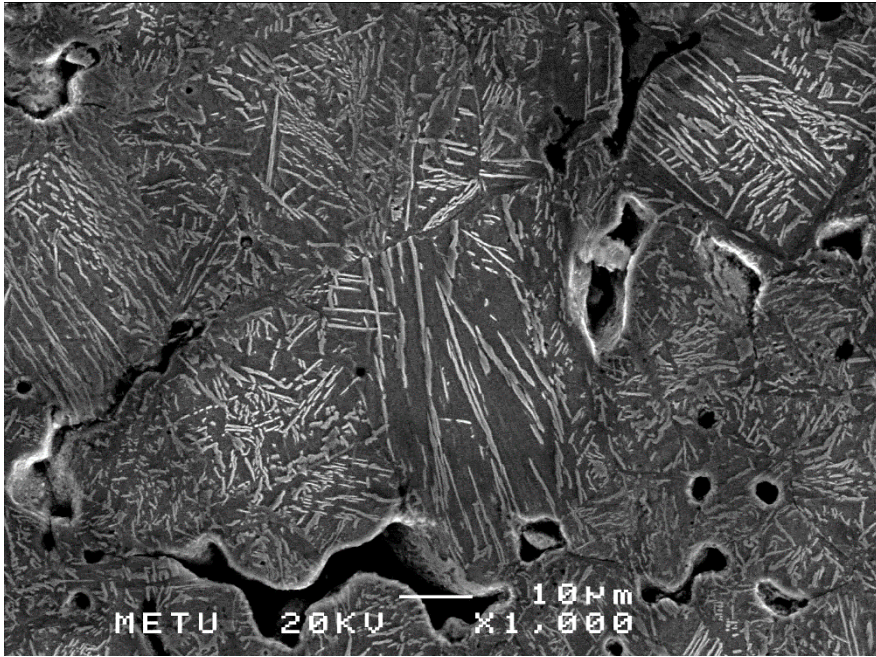


Figure 4.1 SEM micrograph of Distaloy DH in as-sintered condition. Mainly pearlitic microstructure

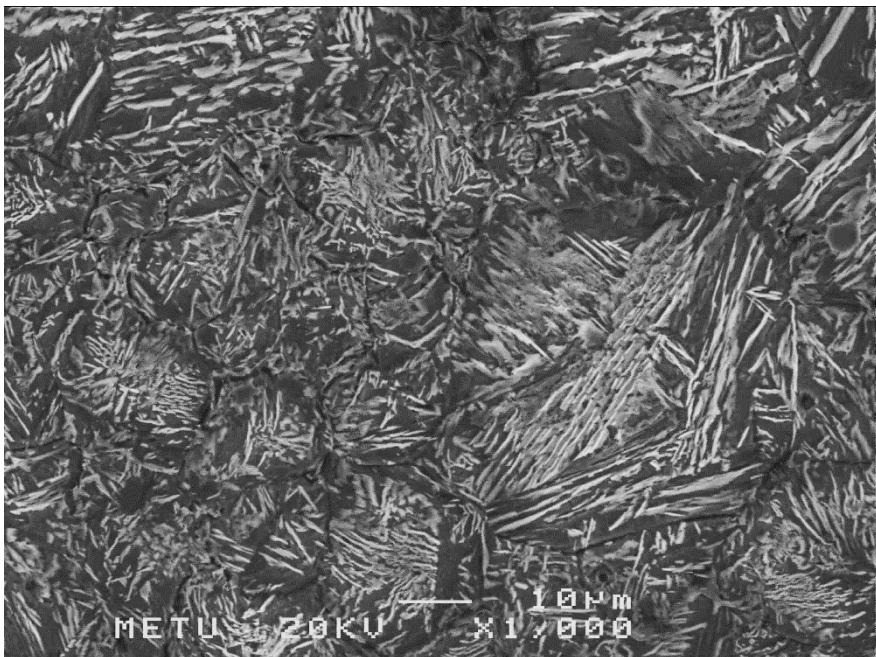


Figure 4.2 SEM micrograph of Astaloy Mo in as-sintered condition. Mainly pearlitic microstructure.

4.1.2 Green Density Measurement

Distaloy-DH and Astaloy Mo powders were compacted under 600 MPa pressure by using tension-compression testing machine with a unidirectional die to get rectangular shape. The green densities of these compacts are computed from the dimensional parameters. Table 4.1 shows the average densities of two components before and after sintering process. As seen, the compacted and sintered densities are very close to each other.

Table 4.1 Average Density values of compacted and sintered Distaloy-DH and Astaloy Mo powders

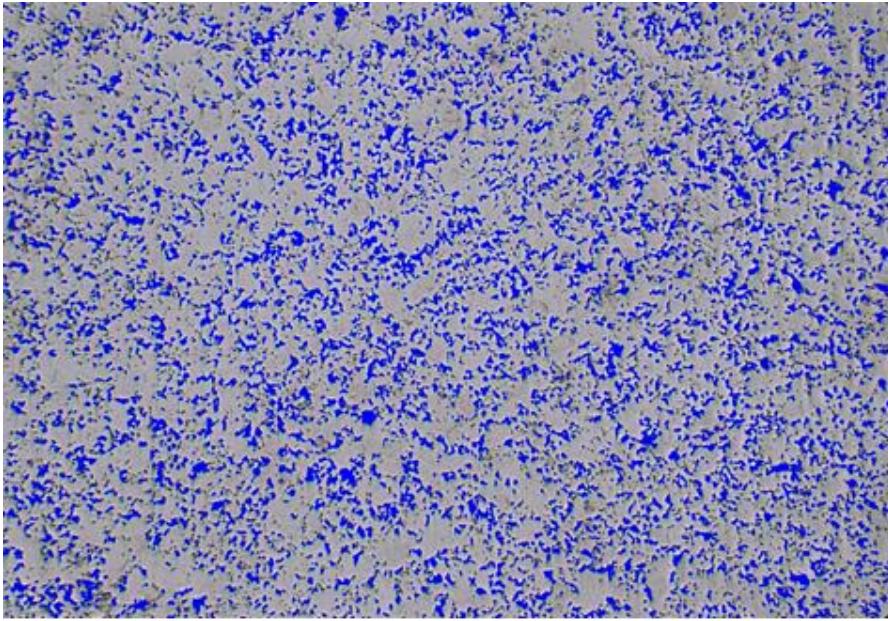
Base powder	Green Density (g/ cm ³)	As sintered Density (g/ cm ³)
Distaloy-DH	6.95 ± 0.04	6.95 ± 0.07
Astaloy Mo	6.93 ± 0.06	6.91 ± 0.06

4.1.3 Porosity Measurement

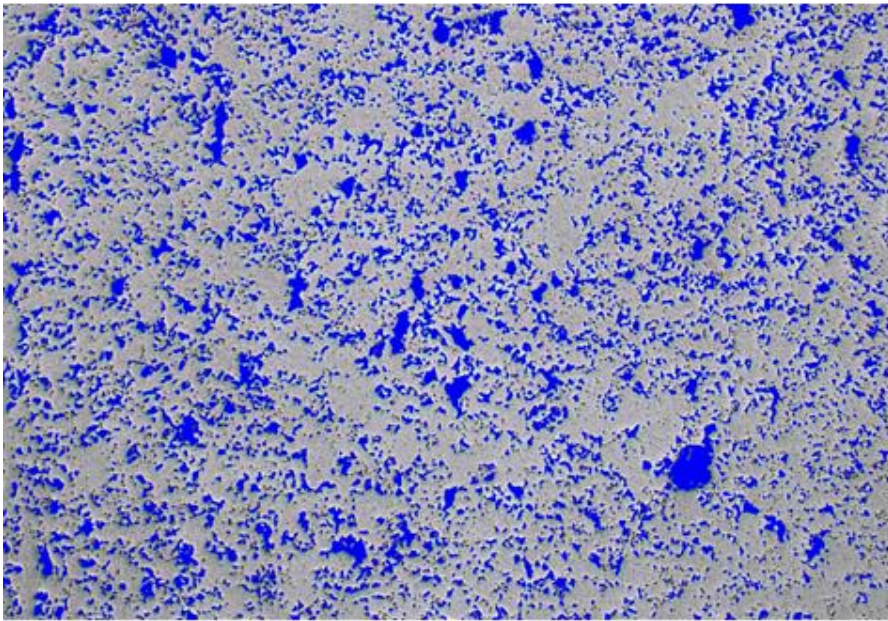
Porosity contents of sintered samples are examined under optical microscope by Image Analyzer Clemex Software. The specimens are in as-polished condition. In examination, the pores are shaded as blue as seen in Figure 4.3. The porosity percent is measured by taking the ratio of pores to total area. Results are shown in Table 4.2.

Table 4.2 The amount of porosity of sintered Distaloy DH and Astaloy Mo specimens

Base powder	Porosity (%)
Distaloy-DH	10.85
Astaloy Mo	12.77



(a)



(b)

Figure 4.3 Pores are shaded as blue in image analyzer Clemex software. a) Sintered Distaloy-DH, b) sintered Astaloy Mo at a magnification of 100X.

4.2 Characterization of Heat Treated Specimens

Different heat treatment cycles are applied to the sintered samples in order to investigate the effect of microstructure on mechanical properties of Distaloy-DH and Astaloy Mo alloys. The microstructure of samples are analyzed by SEM and optical microscopes. In this study, pearlite, martensite and different types of bainite morphologies are obtained depending on the applied heat treatments.

The martensite start (M_s) and bainite start (B_s) temperatures are important in determining the isothermal treatment temperatures. The B_s temperature is generally assumed as the highest temperature where upper bainite is seen. Therefore, a specimen hold just below this temperature will most probably yield upper bainite phase mixture. On the other hand, if a specimen is hold just above the M_s temperature, lower bainite phase mixture should form. In calculation of M_s and B_s temperatures, the following formulas are used [4, 30]:

$$M_s (\text{°C}) = 521 - 353C - 225Si - 24.3Mn - 27.4Ni - 17.7Cr - 25.8Mo \quad (4.1)$$

$$B_s (\text{°C}) = 830 - 270C - 90Mn - 37Ni - 70Cr - 83Mo \quad (4.2)$$

Using equations (4.1) and (4.2), the calculations yield different temperatures. For example, neglecting Cu, the M_s is calculated as 235°C and B_s is 516°C. Due to these calculations, it is safe to assume that an isothermal treatment at 450°C will give an upper bainitic microstructure. On the other hand, an isothermal treatment at 300°C will yield a lower bainitic microstructure. For isothermal treatments, the sintered samples are austenitized at 850°C and then quenched in a salt bath at either 450°C or 300°C for 5 minutes, 15 minutes or 30 minutes.

For comparison purposes, several specimens are either water quenched or normalized as well. The microstructural constituents obtained from different heat treatment cycles are shown in the following sections.

4.2.1 Microstructural Characterization of Normalized and Quenched Distaloy-DH Specimens

Figure 4.4 shows the martensitic microstructure of Distaloy DH after water quenched from 850°C. A fully martensitic microstructure is observed as expected with a needle shape morphology. Figure 4.5 show the pearlite microstructure of sintered Distaloy DH after austenitized at 850°C and air cooled (normalized). The morphology of pearlite seems to be modified due to the presence of Mo.

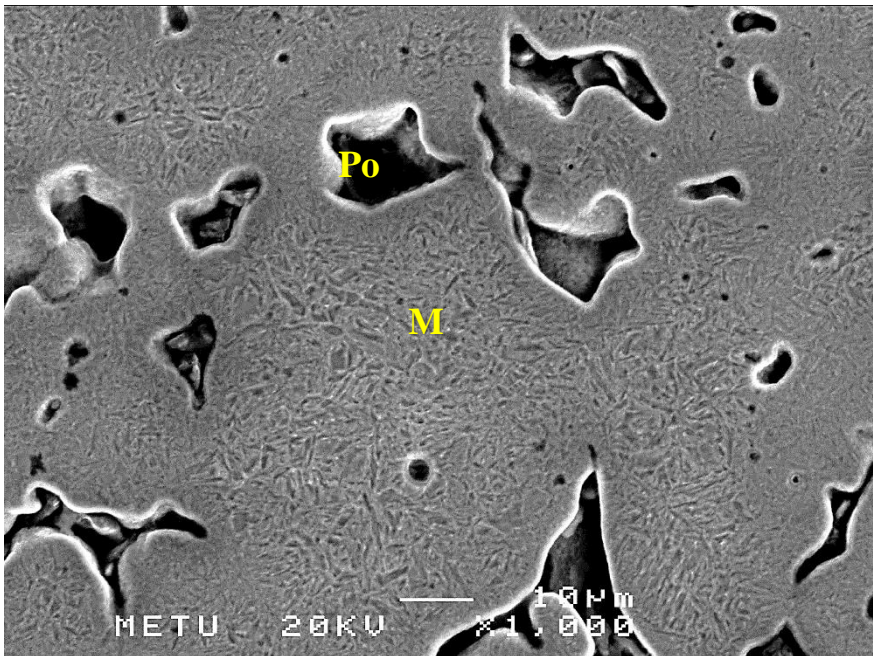


Figure 4.4 The microstructure of Distaloy DH after water quenched and tempered. Martensite (M), Porosity (Po).

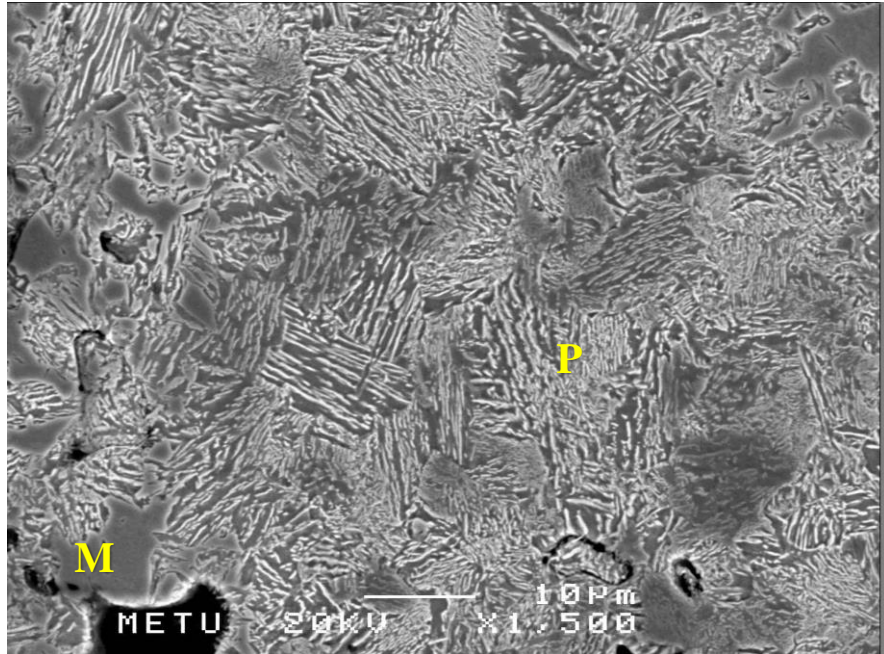


Figure 4.5 The microstructure of Distaloy-DH after normalizing treatment. The microstructure is a mixture of pearlite (P) and martensite (M).

4.2.2 Microstructural Characterization Isothermally Treated Specimens of Distaloy DH

4.2.2.1 Isothermal Treatment of Distaloy DH at 450°C

For upper bainite phase formation, the Distaloy specimens are quenched into the salt bath at 450°C. Samples are hold at that temperature for either 5, 15 or 30 minutes. Figure 4.6 shows lamellar morphology of upper bainite in Distaloy sample after holding 5 minutes at 450°C. The lamellar morphology is seen in Figure 4.7 at a higher magnification.

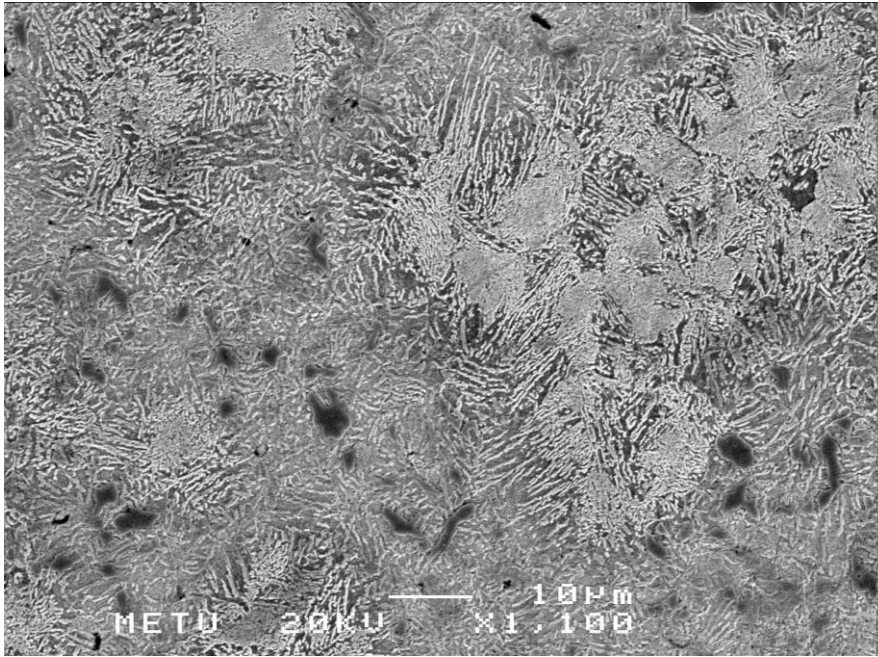


Figure 4.6 SEM micrograph of the Distaloy specimen after an isothermal treatment at 450°C for 5minutes. The microstructure consists of upper bainite

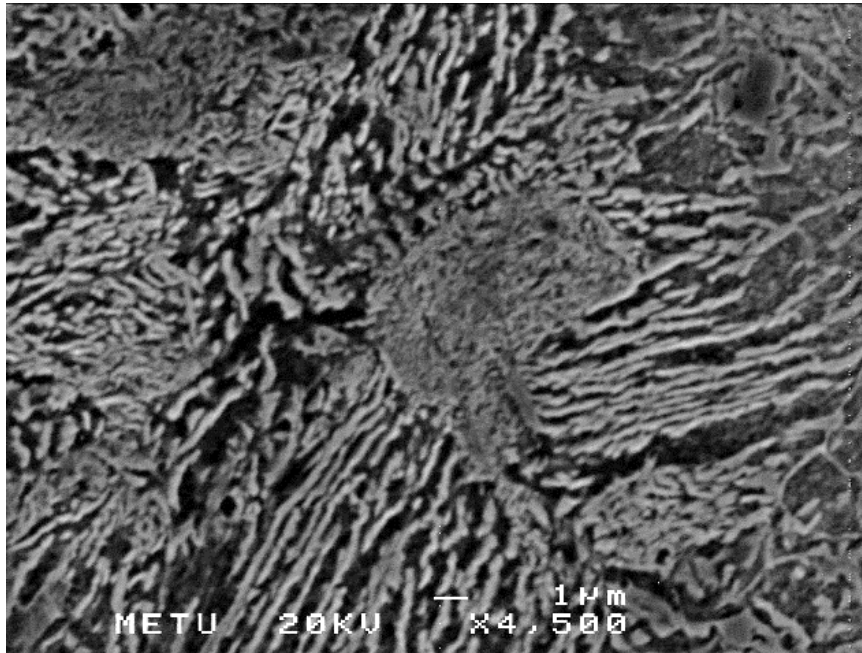


Figure 4.7 SEM micrograph of the Distaloy specimen after an isothermal treatment at 450°C for 5minutes. Upper bainite at a higher magnification.

Distaloy DH samples isothermally treated at 450°C for 15 and 30 minutes shows similar results to that of 5 minutes samples. As seen in Figure 4.8 and Figure 4.9, the upper bainite dominates the microstructure uniformly. Bainite sheaves of samples isothermally heat treated for 30 minutes shows thicker layers of ferrite than samples with same heat treatment for 5 minutes.

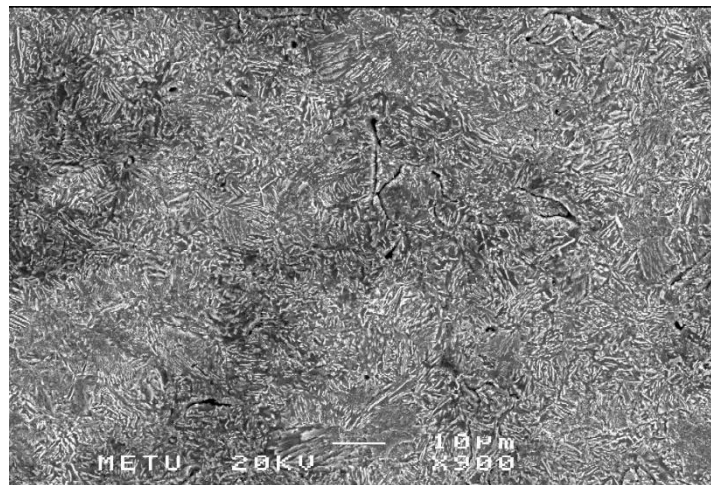


Figure 4.8 SEM micrograph of the Distaloy specimen after an isothermal treatment at 450°C for 30 minutes at a magnification of 900X.

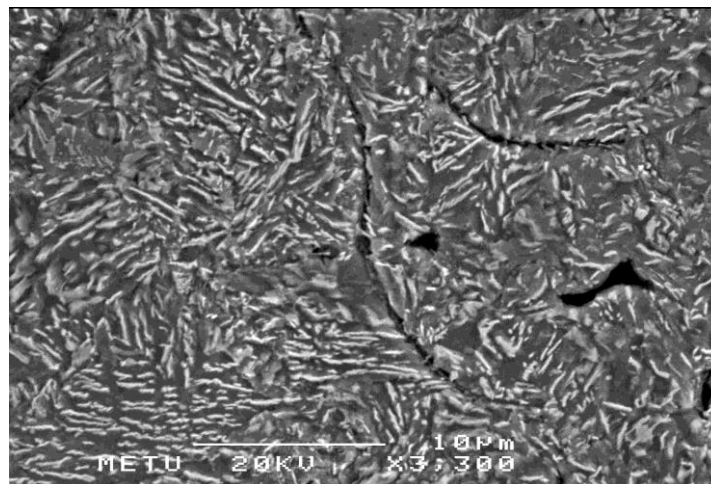


Figure 4.9 SEM micrograph of the Distaloy specimen after an isothermal treatment at 450°C for 30 minutes.

4.2.2.2 Isothermal Treatment of Distaloy DH at 300°C

By deriving M_s value from equation 4.1, isothermal heat treatment on sintered sample at 300°C is done after austenitizing them at 850°C to obtain the morphology of lower bainite in Distaloy-DH. Figure 4.10 shows a general view of Distaloy sample isothermally heat treated at 300°C for 5 minutes. In the same specimen, both martensite and bainite phases are seen. An important point here is that the bainitic reaction is not complete after 5 minutes of isothermal treatment at 300°C.

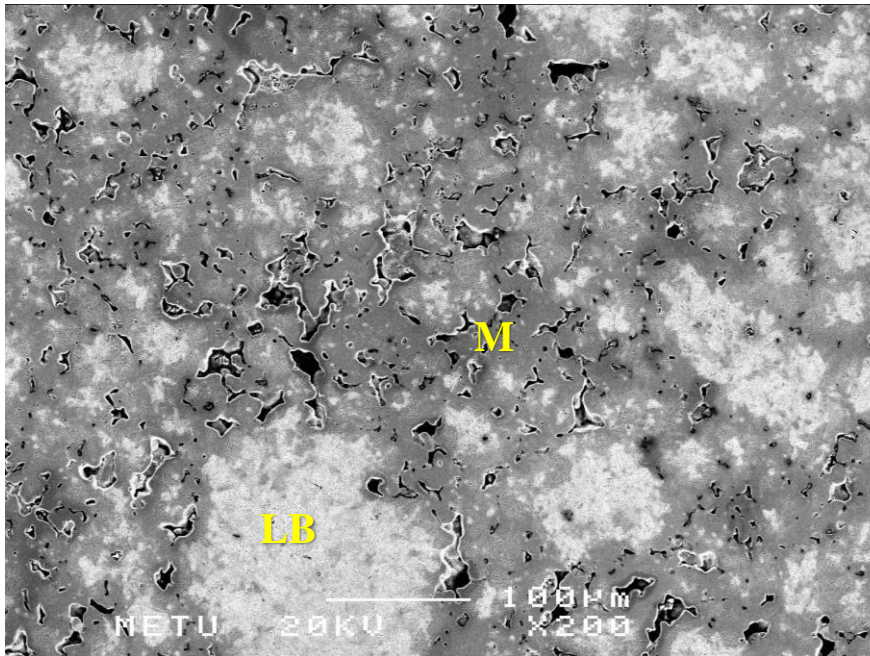
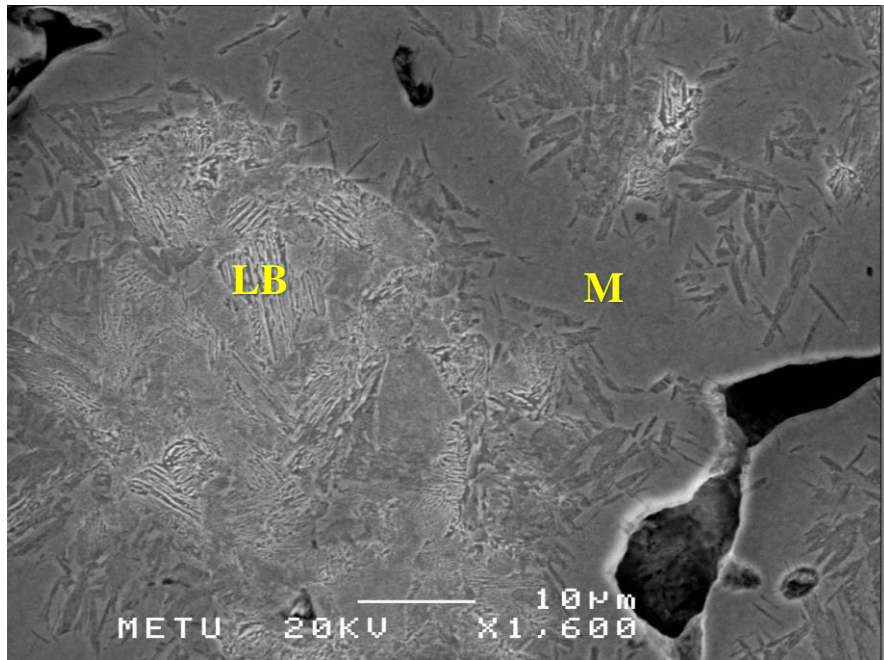
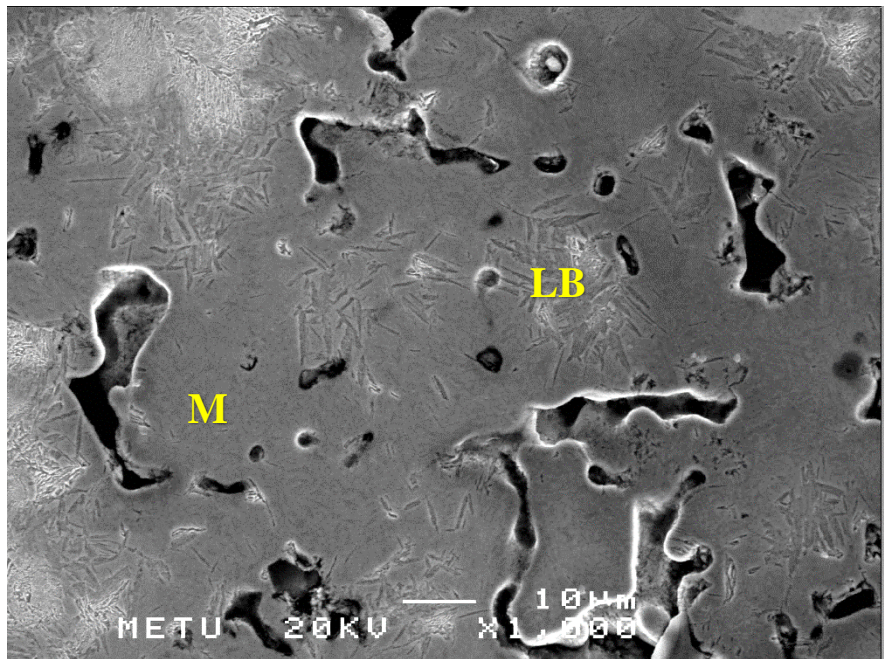


Figure 4.10 SEM micrograph of the Distaloy specimen after an isothermal treatment at 300°C for 5 minutes. Microstructure is a mixture of Lower Bainite and martensite.



(a)



(b)

Figure 4.11(a) and (b) SEM micrograph of the Distalloy specimen after an isothermal treatment at 300°C for 5 minutes. Lower Bainite (LB), Martensite (M).

Figure 4.11 (a) and (b) show the microstructure of the same sample at a higher magnification. There are martensite islands in the microstructure as well. As nital etches the bainite phase more rapidly than martensite, the martensite islands do not show the acicular morphology. At definite regions, the amount of martensite is very low (Figure 4.12).

The morphology of bainite is in more acicular form when compared to upper bainite. The morphological variation of the bainite sheaves are given in Figure 4.13 to Figure 4.15 at high magnifications (around 20,000X) the lamellar carbide precipitation in lower bainite can be seen very clearly (Figure 4.14). When upper and lower bainite microstructures for Distaloy DH samples are compared, it can be concluded samples with lower bainite have a much finer microstructure than upper bainite.

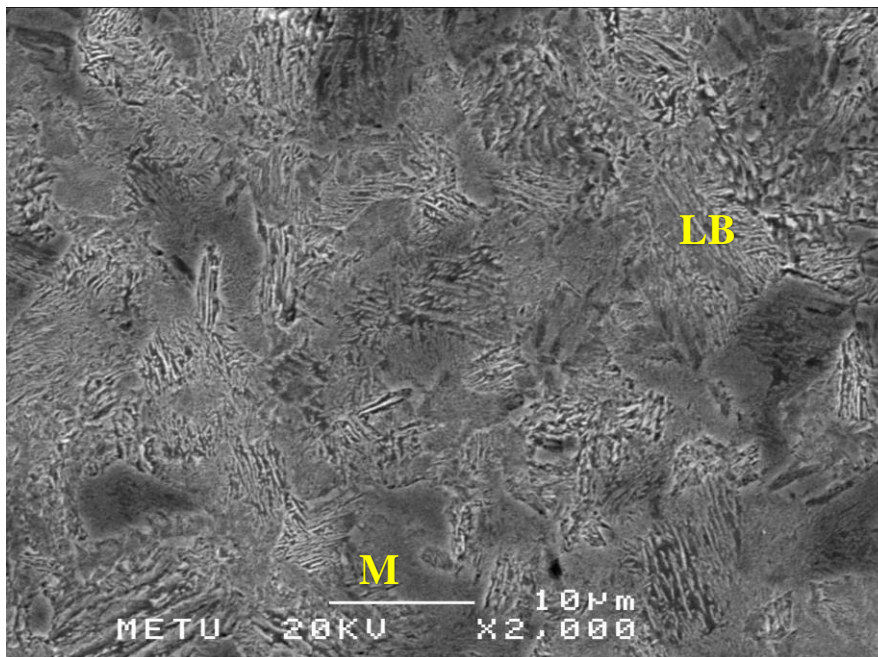


Figure 4.12 SEM micrograph of the Distaloy specimen after an isothermal treatment at 300°C for 5 minutes. Lower Bainite(LB),Martensite,

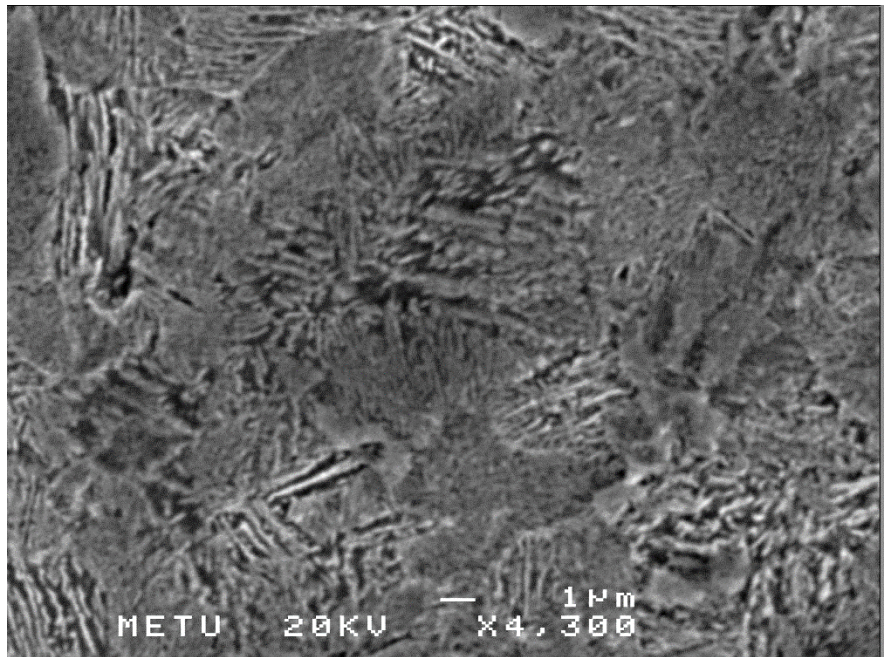


Figure 4.13 SEM micrograph of the Distaloy specimen after an isothermal treatment at 300°C for 5 minutes with higher magnification

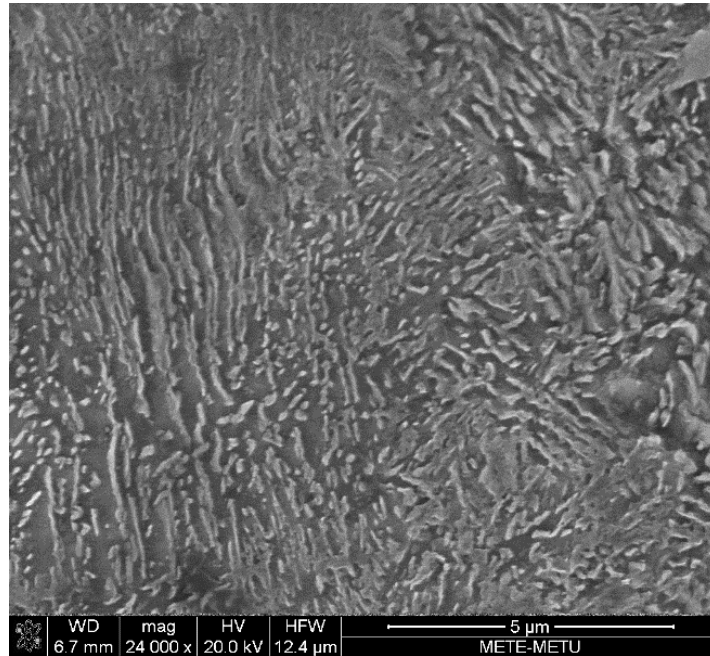


Figure 4.14 SEM micrograph of the Distaloy specimen after an isothermal treatment at 300°C for 5 minutes at a magnification of 24,000X with a bainitic morphology

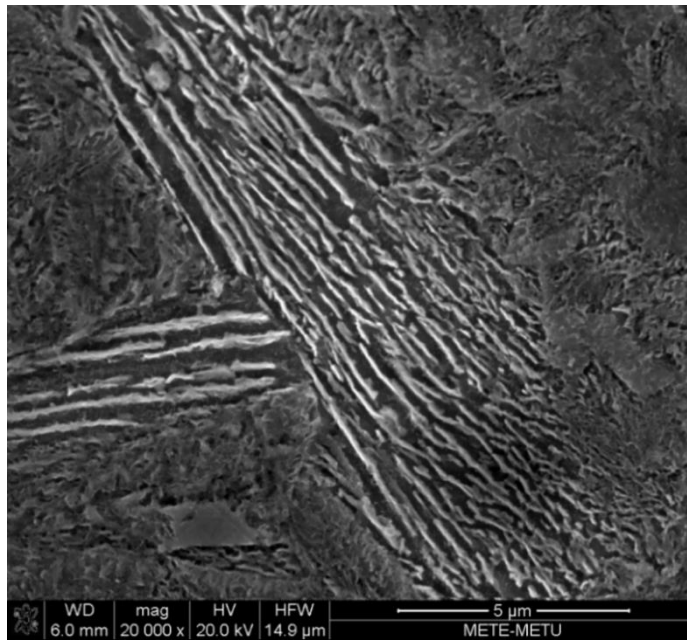


Figure 4.15 SEM micrograph of Distalloy Isothermal cooled at 300°C for 30 minutes. Lower bainite at 20000X magnification. Two different morphologies are seen.

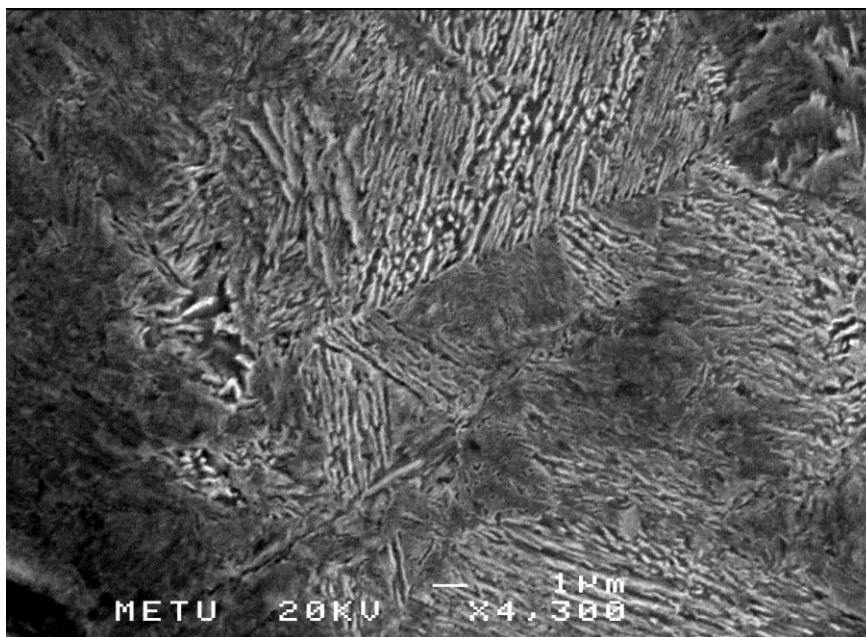


Figure 4.16 SEM micrograph of Distalloy Isothermal cooled at 300°C for 30 minutes. The bainite sheaves are seen clearly.

An image analysis is done on isothermally heat treated samples in order to determine the amount of martensite left after an isothermal treatment at 300°C for 5 and 15 minutes. In this thesis study, selective etching by 2% Nital etchant is applied to determine the volume fraction of bainite in the samples. Bainite develops at an earlier stage with respect to martensite when etched with 2% Nital. Using selective etching, the bainitic regions in the samples were developed and the volume fraction of the bainite phase is calculated using CLEMEX image analyzer software. As can be seen in Figure 4.17, bainitic regions are shaded red and pore are shown as blue. Table 4.3 reveals that the amount of martensite decreases with an increase in isothermal heat treatment period from 5 minutes to 15 minutes.

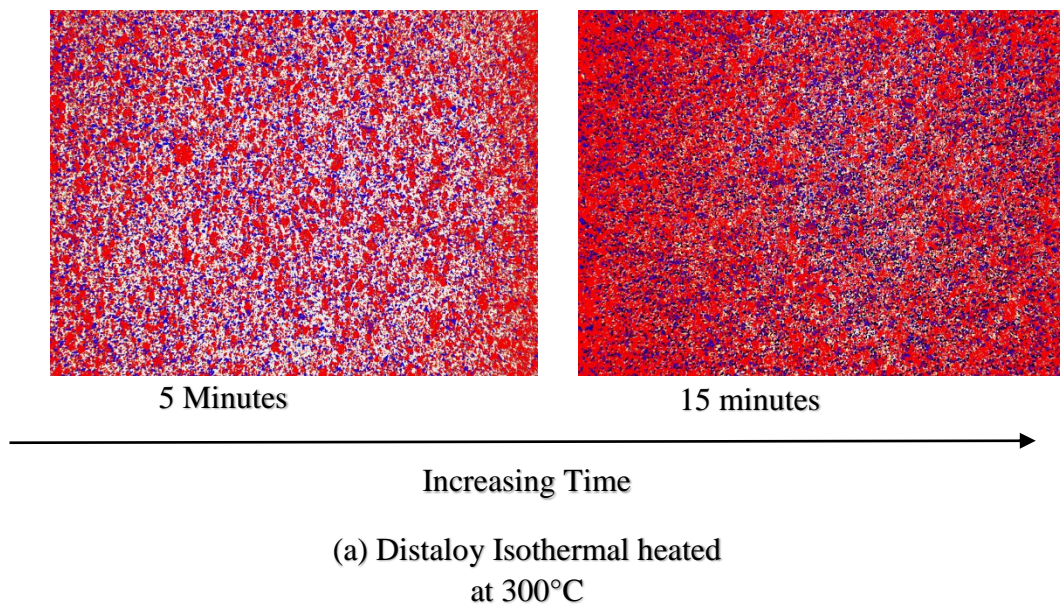


Figure 4.17 The change in bainite and martensite content with increasing time of Distalloy

Table 4.3 Amount of martensite in isothermally treated samples of Distaloy DH at 300°C.

Isothermal cooled sample at 300°C	Martensite (%) after 5 minutes	Martensite (%) after 15 minutes	Martensite (%) after 30 minutes
Distaloy DH	45.1 ± 6.1	25.3 ± 6.8	0

4.2.3 Microstructural Characterization of Normalized and Quenched Astaloy Mo Specimens

This powder has the same composition with that of Distaloy DH but copper is added by admixing method. Microstructure of normalized and water quenched samples are very similar to that of Distaloy. Figure 4.18 shows the needle shape microstructure of martensite islands in quenched specimen. Figure 4.19 and Figure 4.20 show the pearlite microstructure of Distaloy DH after austenitized at 850°C and air cooled (normalized). The morphology of pearlite seems to be modified due to the presence of Mo. However, upper bainite can also present at definite locations, which has a very similar structure to pearlite.

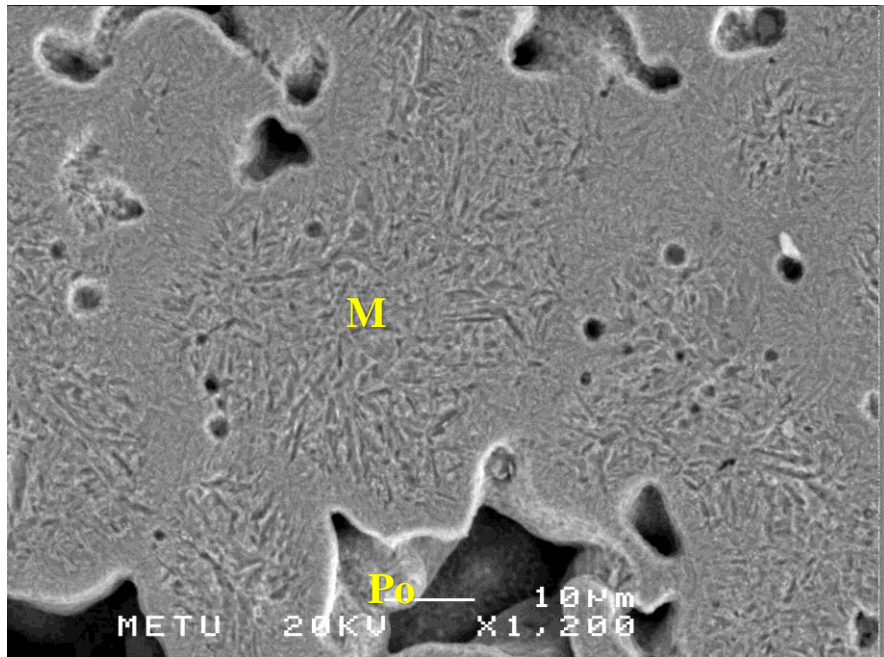


Figure 4.18 The microstructure of Astaloy Mo after water quenched and tempered. Martensite (M), Porosity (Po). Only martensite phase is seen.

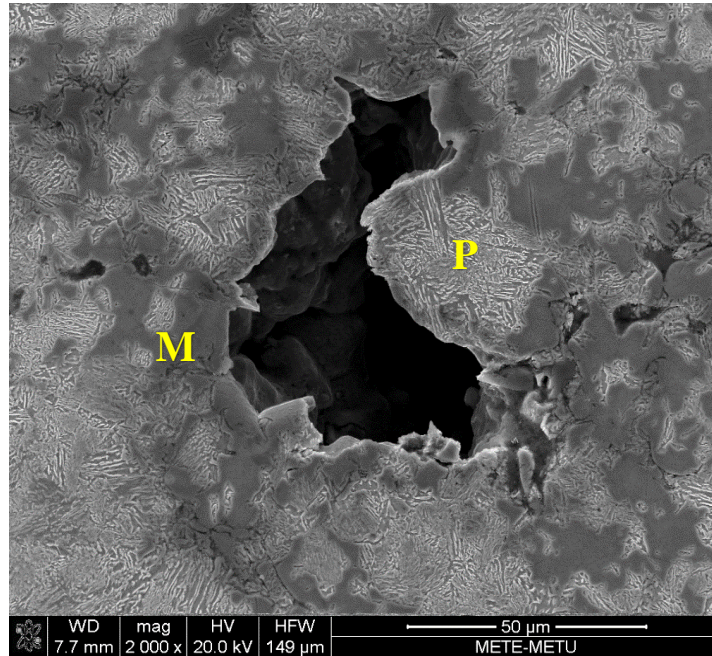


Figure 4.19 Pearlite and martensite phases in Astaloy specimen after a normalizing treatment. Martensite (M), Pearlite (P).

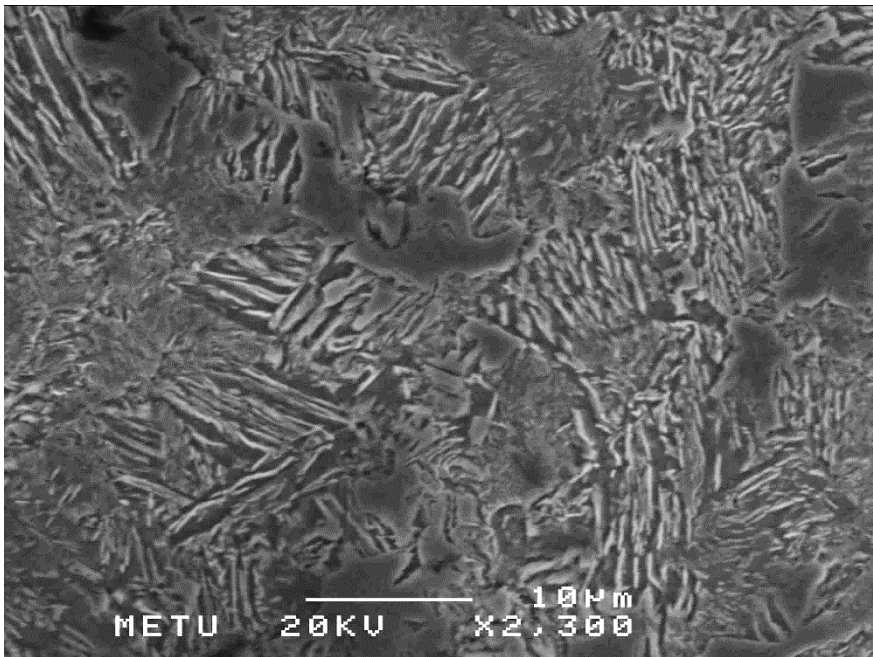


Figure 4.20 The microstructure of Astaloy Mo after normalizing treatment.

4.2.4 Microstructural Characterization Isothermally Treated Specimens of Astaloy Mo

4.2.4.1 Isothermal Treatment of Astaloy Mo at 450°C

As it was mentioned previously Astaloy and Distaloy have the same composition. Therefore, B_s and M_s of Astaloy should be identical to that of Distaloy. For upper bainite phase formation, the Astaloy specimens are quenched into the salt bath at 450°C. Samples are hold at that temperature for either 5, 15 or 30 minutes. Figure 4.21 illustrates bainitic microstructure of sample with fine lamellar upper bainite (lamellar ferrite sheaves). Sample has a very similar microstructure observed in Distaloy with same isothermal heat treatment.

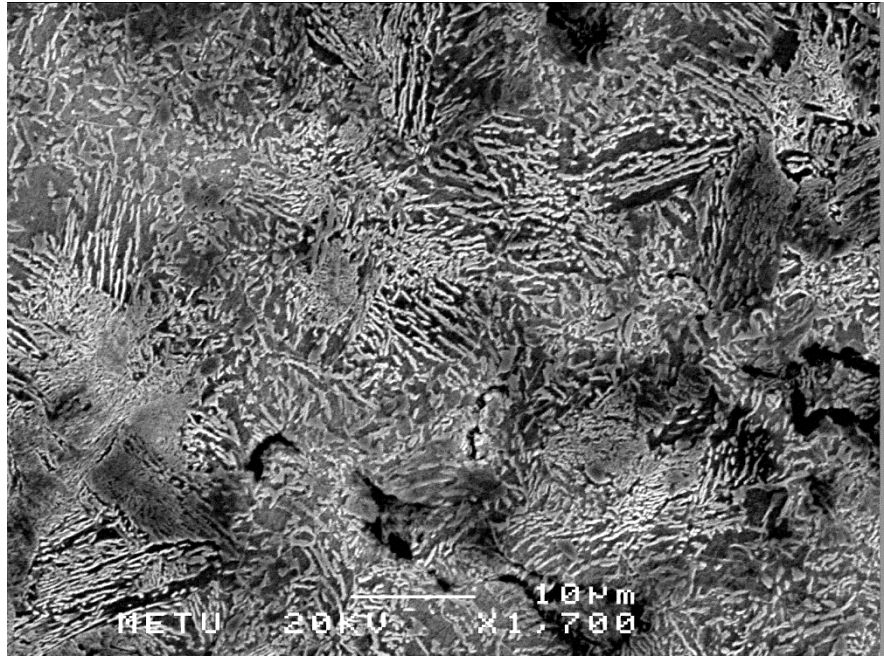


Figure 4.21 SEM micrograph of the Astalloy specimen after an isothermal treatment at 450°C for 5 minutes with mainly Upper Bainitic morphology.

The upper bainite in Astalloy specimens can be seen at different morphologies (Figure 4.21, Figure 4.22, Figure 4.23). This can be due to that admixed Cu is not distributed homogeneously.

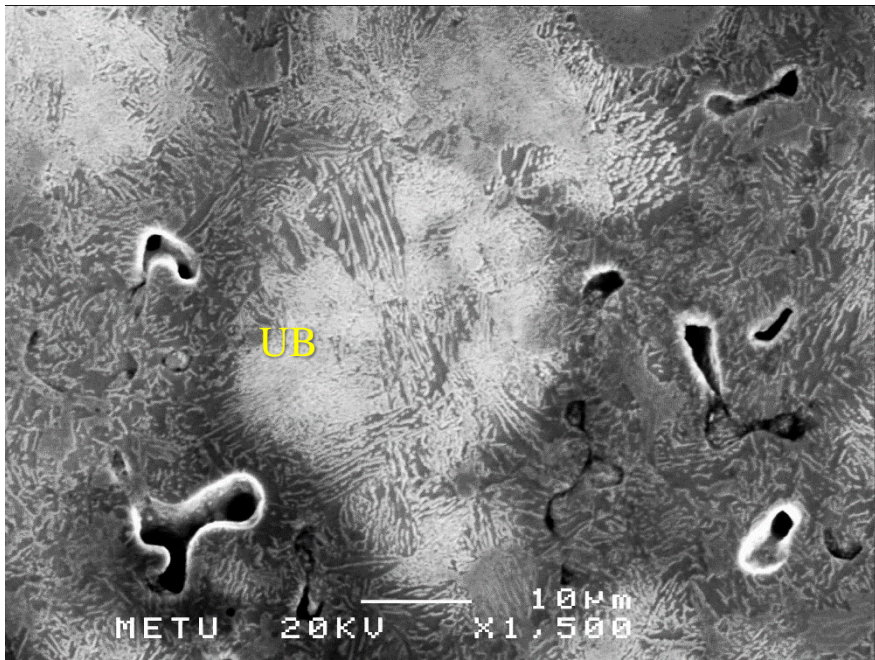


Figure 4.22 SEM micrograph of the Astaloy specimen after an isothermal treatment at 450°C for 30 minutes

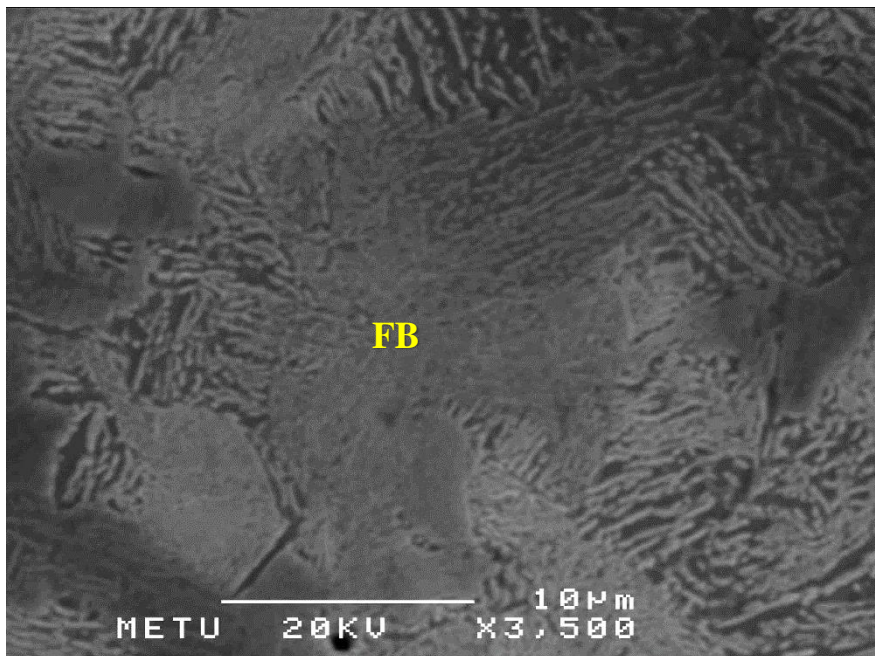


Figure 4.23 SEM micrograph of Astaloy Mo Isothermal cooled at 450°C for 30 minutes. At definite regions, the lamellar structure is very fine. fine Lamellar bainite(FB).

4.2.4.2 Isothermal Treatment of Astaloy Mo at 300°C

By deriving M_s value from equation 4.1, isothermal heat treatment on sintered at 300°C is done after austenized them at 850°C to obtain the morphology of lower bainite in Astaloy Mo. Figure 4.24 shows a general view of Astaloy sample isothermally heat treated at 300°C for 5 minutes. The microstructure consists of a mixture of lower bainite and martensite. As seen in Figure 4.25, the bainite phase is in the form of islands within martensite phase. Therefore, it can be stated that in Astaloy specimens, a treatment of 5 minutes is not enough to transform all the austenite to bainite.

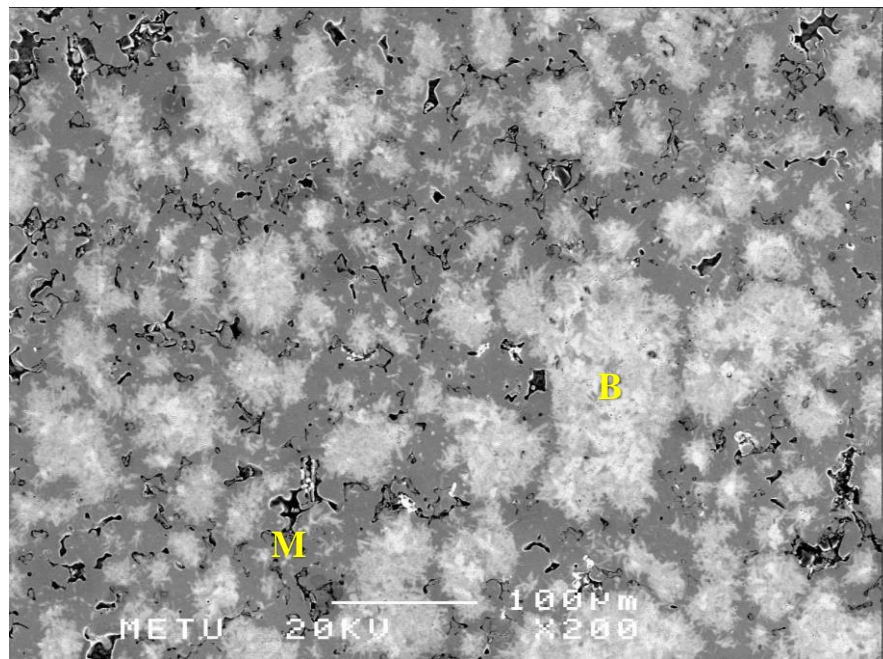


Figure 4.24 SEM micrograph of the Astaloy specimen after an isothermal treatment at 300°C for 5 minutes

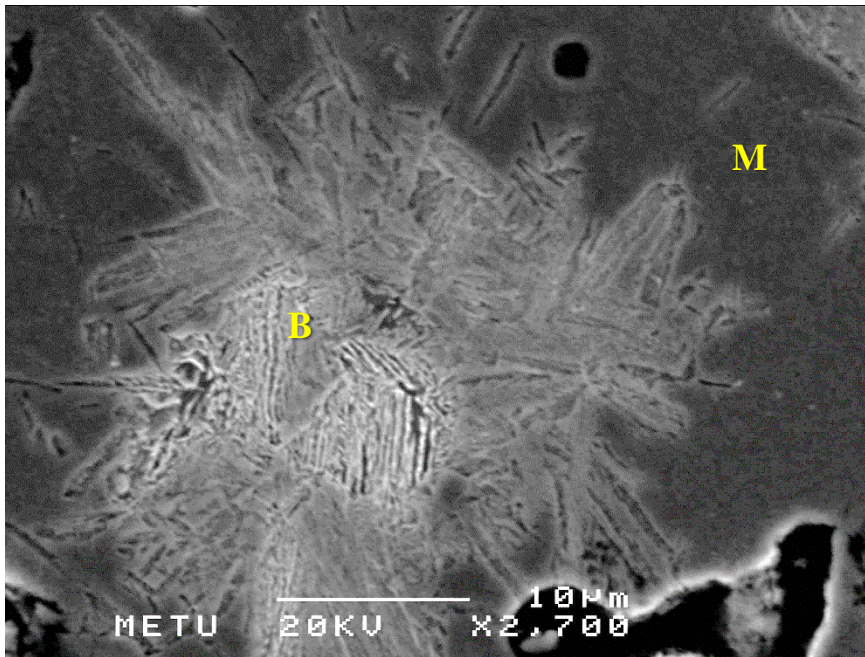


Figure 4.25 SEM micrograph of the Astaloy specimen after an isothermal treatment at 300°C for 5 minutes. Martensite (M) and two different morphologies of bainite are observed.

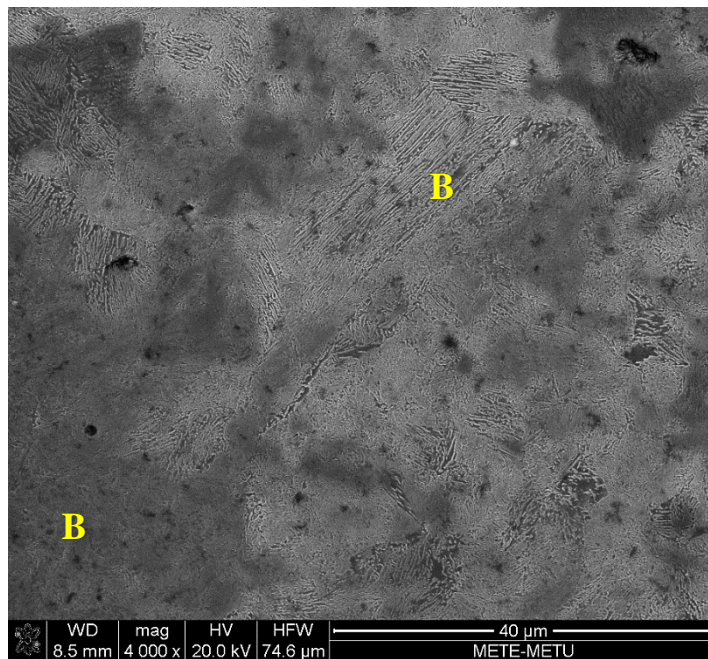


Figure 4.26 SEM micrograph of the Astaloy specimen after an isothermal treatment at 300°C for 30 minutes.

For samples with same isothermal heat treatment at 300°C for 30 minutes, only lower bainite phase is observed (Figure 4.27, Figure 4.28).

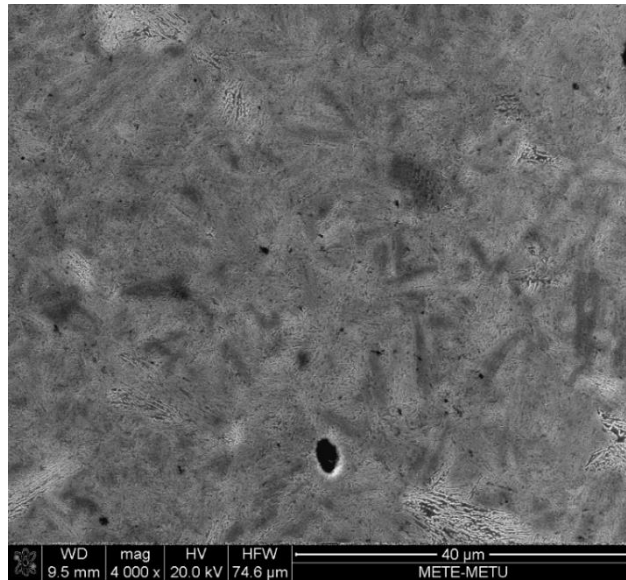


Figure 4.27 SEM micrograph of the Astalloy specimen after an isothermal treatment at 300°C for 30 minutes.

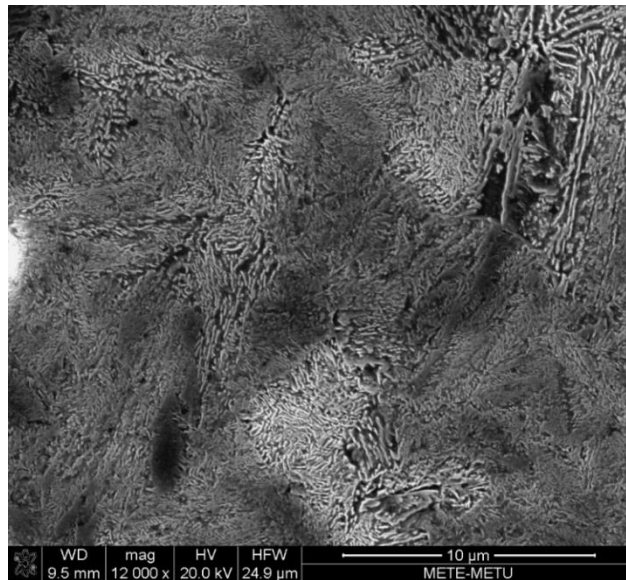


Figure 4.28 SEM micrograph of the Astalloy specimen after an isothermal treatment at 300°C for 30 minutes. Lamellar bainite morphology is seen (12000X magnification).

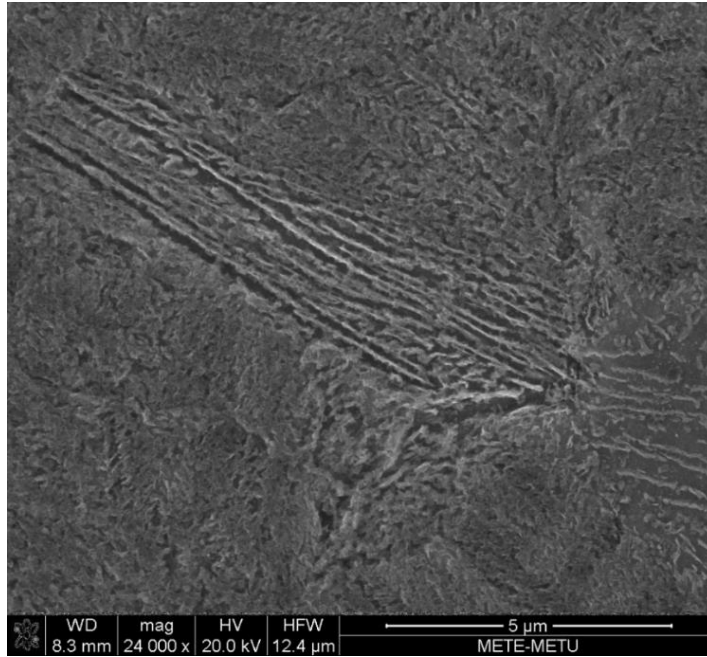


Figure 4.29 SEM micrograph of the Astaloy specimen after an isothermal treatment at 300°C for 30 minutes. Morphology of lower bainite with high resolution(24,000X).

Image analysis is done on isothermally heat treated samples of Astaloy similar to Distaloy in order to determine the amount of martensite left after an isothermal treatment at 300°C for 5 and 15 minutes. The bainitic regions in the samples were developed and the volume fraction of the bainite phase is calculated using CLEMEX image analyzer software. The results of image analysis are shown in Figure 4.30, bainitic regions are shaded red and pore are shown as blue. Table 4.4 reveals that the amount of martensite decreases with an increase in isothermal heat treatment period from 5 minutes to 15 minutes for Astaloy Mo as well as Distaloy-DH.

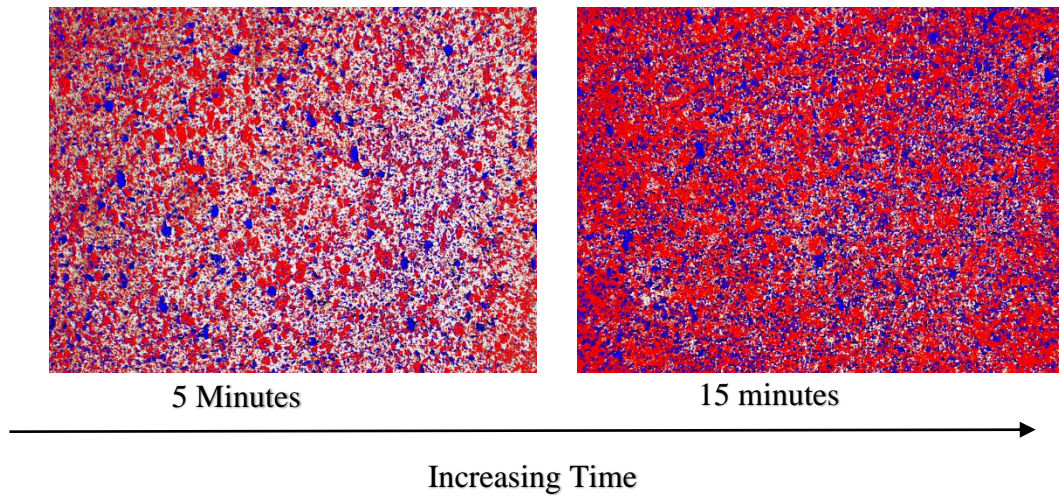


Figure 4.30 The change in bainite and martensite content of isothermal treated Astaloy at 300°C with increasing time

Table 4.4 Amount of martensite in isothermally treated samples of Astaloy Mo at 300°C.

Isothermal cooled sample at 300°C	Martensite (%) after 5 minutes	Martensite (%) after 15 minutes	Martensite (%) after 30 minutes
Astaloy	48.3 ± 6.3	18.0 ± 2.0	0

As a concluding remark, all the phases detected in the specimens are summarized in Table 4.5. The transition from pearlite phase to martensite and lower bainite or upper bainite phases at different heat treatments is observed in the samples. (“P” is pearlite, “UB” is Upper bainite, “LB” is Lower bainite and “M” is martensite.)

Table 4.5 Summary of phases observed in sintered and austenitized Distaloy DH and Astaloy Mo samples with various heat treatments

Samples	Heat Treatment							
	Isothermal Heat treatment						WQ	Air cool
	300°C			450°C				
	5min	15min	30min	5min	15min	30min		
Distaloy DH	“M” and “LB”	“M” and “LB”	“LB”	“UB”	“UB”	“UB”	“M”	“M” and “P”
Astaloy Mo	“M” and “LB”	“M” and “LB”	“LB”	“UB”	“UB”	“UB”	“M”	“M” and “P”

4.3 Hardness Measurements of As-Sintered and Heat Treated Specimens

Macrohardness measurements are done for both as-sintered and heat treated samples. The hardness values are tabulated in Table 4.6 and plotted in Figure 4.31 and Figure 4.32. When examined it is seen that the hardness value of the Distaloy specimen is around 187.5 HB after sintering. A normalizing treatment does not increase the hardness values considerably and yields an average value of 196.3 HB. In order to compare the hardness values of bainitic specimens with that of martensitic specimens, several specimens are quenched in water. A quenching operation yields a hardness of 396.5 HB. After a tempering operation at 180°C, the hardness is dropped to 358.5 HB as expected. Isothermal heat treated samples at 300°C gives higher hardness values than the samples treated at 450°C. The hardnesses of the samples transformed at 300°C, are in the range 260-302 HB, whereas that of 450°C, are in the range 177-186

HB. This can be attributed to the presence of lower and upper bainitic structures. However, it must be noted that for specimens transformed at 300°C, the hardness values decrease from 302HB to 260HB as the time in salt bath is increased from 5minutes to 30minutes. It is believed that this is due to the presence of martensite phase together with lower bainite at short treatment times.

The quenched, quenched and tempered specimens yield higher hardness values with respect to lower bainitic specimens.

The trend in hardness values of the Astaloy specimens are very similar to that of Distaloy. The quenched, quenched and tempered samples shows hardness values in the range of 387-410HB which is higher than isothermally cooled samples at 300°C yielded the hardness values in the range of 175-275HB. In addition, samples treated at 450°C yield lower values of hardness. Only the hardness of the specimen treated at 450°C for 5mins is unexpectedly higher.

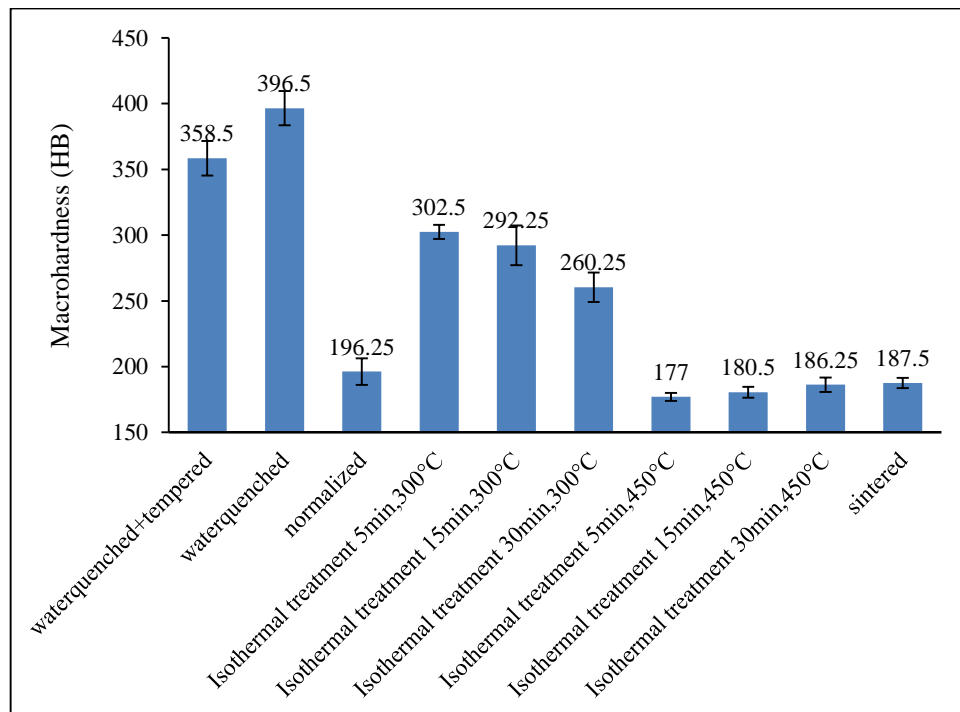


Figure 4.31 Macrohardness values of Distaloy DH with varying heat treatments

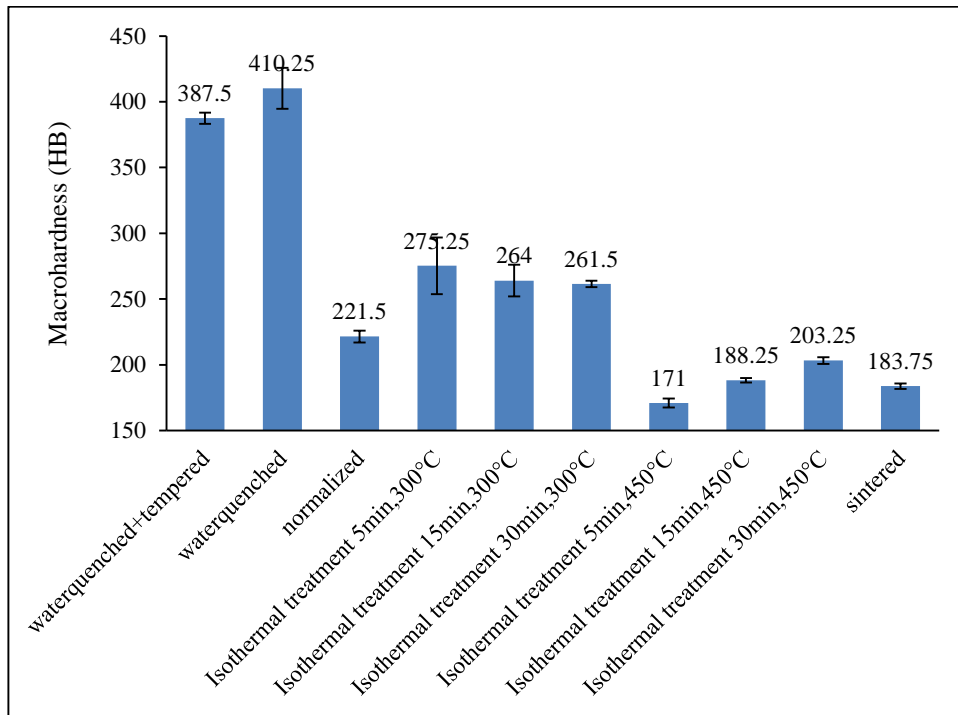


Figure 4.32 Macrohardness values of Astaloy Mo with varying heat treatments

Table 4.6 Macrohardness values of Distaloy-DH and Astaloy Mo with varying heat treatments

Applied Heat treatments on sintered Samples	Average of Hardness (HB)									
	300°C			450°C			Sintered	Air cool	WQ	WQ+Temper
	5 min	15min	30min	5min	15min	30min				
Distaloy DH	302.5±5.3	292.2±15.1	260.2±11.1	177±2.9	180.5±4.0	186.2±5.4	187.5±3.8	196.2±10.1	396.5±13.0	358.5±13.1
Astaloy Mo	275.25±21.6	264±12.0	175.2±8.7	252.2±14.8	188.2±1.7	203.2±2.5	183.7±2.0	221.5±4.5	410.25±15.6	387.5±4.2

4.4 Transverse Rupture Strength Measurements of As-Sintered and Heat Treated Specimens

TRS measurements are done for both as-sintered and heat treated samples. The TRS values are tabulated in Table 4.7 and plotted in Figure 4.33 and Figure 4.34. When examined it is seen that the TRS value of the Distaloy specimen is around 1100 MPa after sintering. A normalizing treatment does not increase the hardness values considerably and yields an average value of 1120 MPa. In order to compare the TRS values of bainitic specimens with that of martensitic specimens, several specimens are quenched in water. A quenching operation yields a TRS value of 1060 MPa. After a tempering operation at 180°C, the TRS is increased to 1310 MPa as expected. Isothermal heat treated samples at 300°C gives higher TRS values than the samples treated at 450°C. The TRS of the samples transformed at 300°C, are in the range of 1300-1450 MPa, whereas that of 450°C, have an average value of 1100MPa. This can be attributed to the presence of lower and upper bainitic structures. However, it must be noted that specimens transformed at 450°C, have close values to the sintered and normalized samples. A similar trend is also observed for Astaloy Mo specimens such that the TRS values of martensitic and lower bainitic specimens are 1345MPa and 1290MPa respectively. Moreover, sample treated at 450°C and normalized and sintered show similar TRS values around 1100MPa.

Transverse rupture strength (TRS) values shows that both Astaloy and Distaloy samples with either upper or lower bainitic microstructures, yield very close values to martensitic samples. As seen in Table 4.7, average TRS value of Distaloy (300°C, 15min) is even higher than quenched and tempered sample.

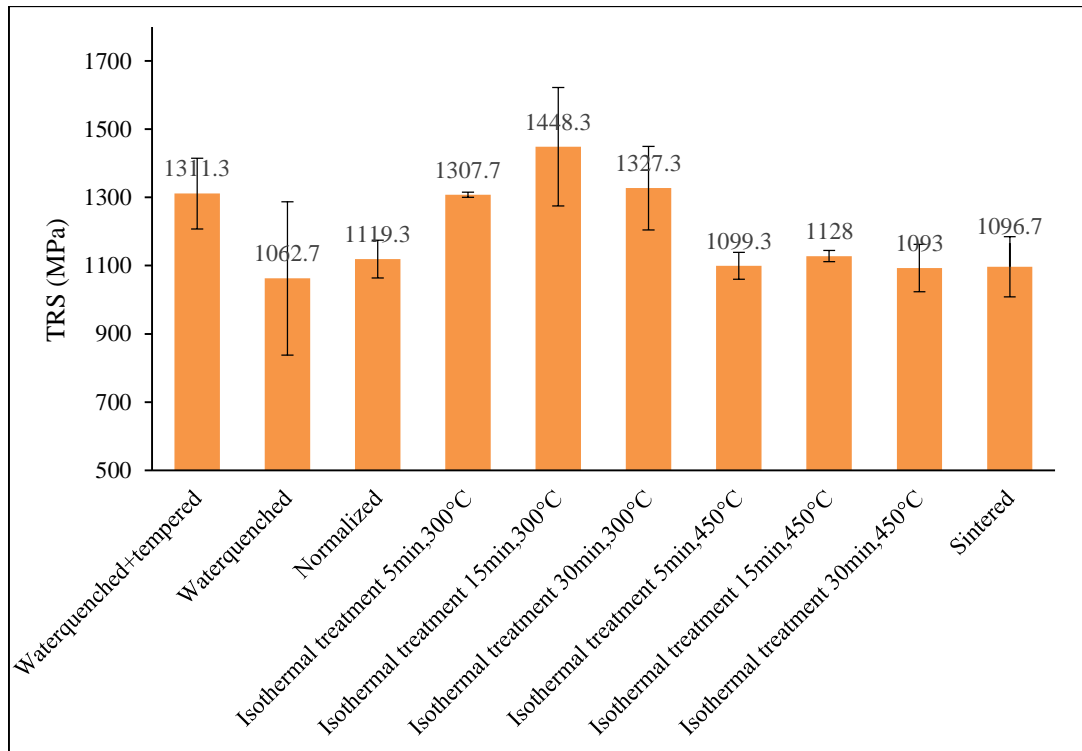


Figure 4.33 TRS values of Distaloy DH with varying Heat treatments.

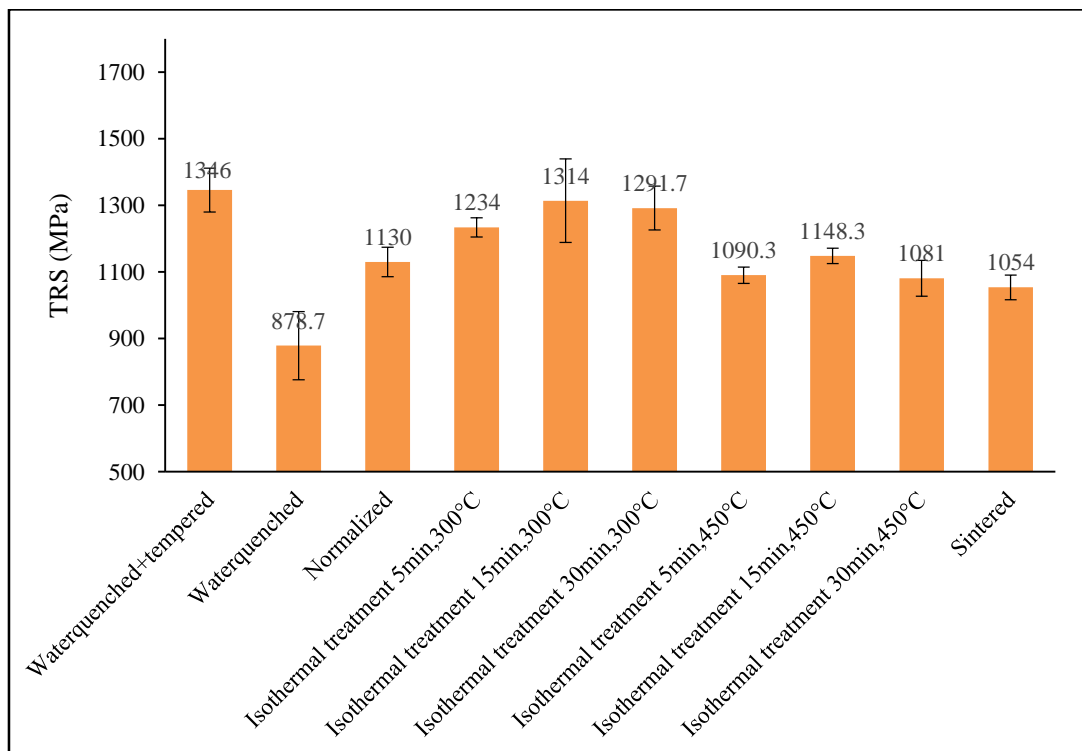


Figure 4.34 TRS values of Astaloy Mo with varying Heat treatments.

Table 4.7 TRS values of Distaloy-DH and Astaloy Mo with varying heat treatments

Applied Heat treatments on sintered Samples	Average of TRS (MPa)									
	300°C			450°C			Sintered	Air cool	WQ	WQ+Temper
	5min	15min	30min	5min	15min	30min				
Distaloy DH	1307.7±7.5	1448.3±173.5	1327.3±122.4	1099.3±39.3	1128±16.7	1093±69.4	1096.7±88.1	1119.3±55.1	1062.7±224.9	1311.3±103.5
Astaloy Mo	1234±29.1	1314±125.1	1291.7±66.0	1090.3±24.3	1148.3±23.2	1081±53.6	1054±37.0	1130±43.8	878.7±102.0	1346±65.9

Figure 4.35, Figure 4.36 and Figure 4.37 compare the TRS values of same samples for both Distaloy and Astaloy. It seems when TRS values of both alloys are compared, samples like isothermally heat treated at 300°C and water quenched tempered shows significant differences than others. On other hand these sample have the highest values.

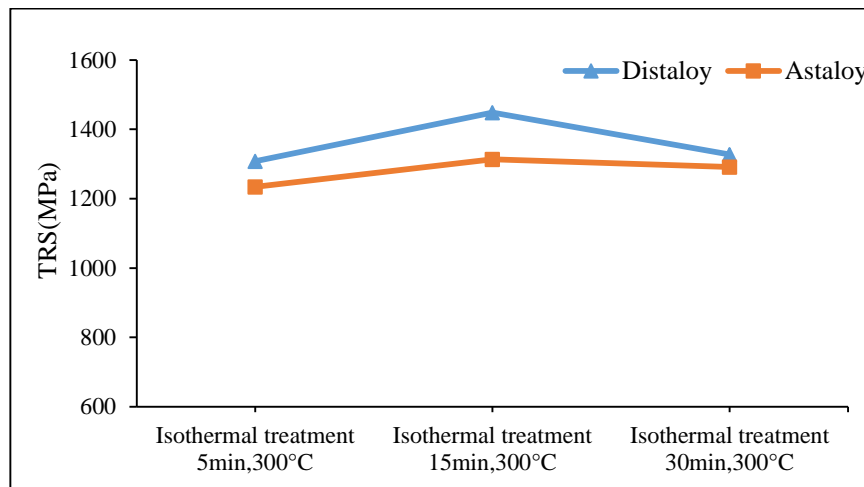


Figure 4.35 Comparison of TRS values for Distaloy and Astaloy of Isothermally heat treated at 300°C with varying times.

Samples isothermally heat treated at 450°C shows a pretty good conformity in values. It also seen normalized and sintered sample values of both Distaloy-DH and Astaloy Mo are pretty close to each other.

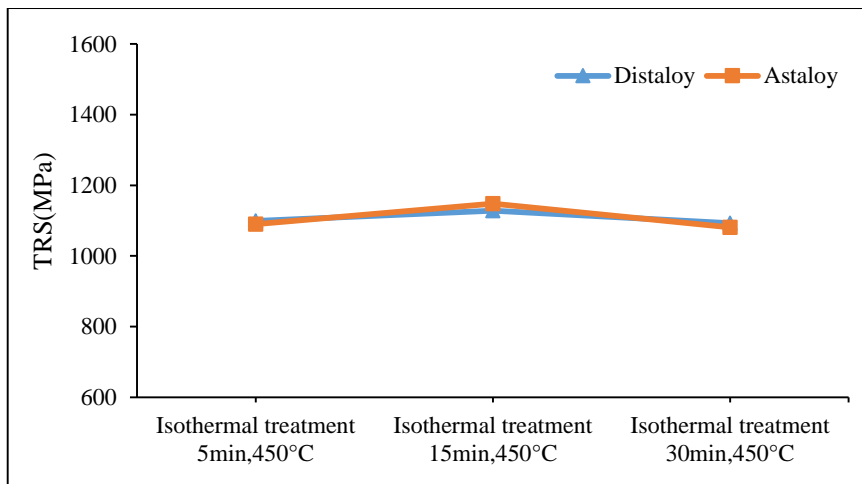


Figure 4.36 Comparison of TRS values for Distaloy and Astaloy of Isothermally heat treated at 450°C with varying times.

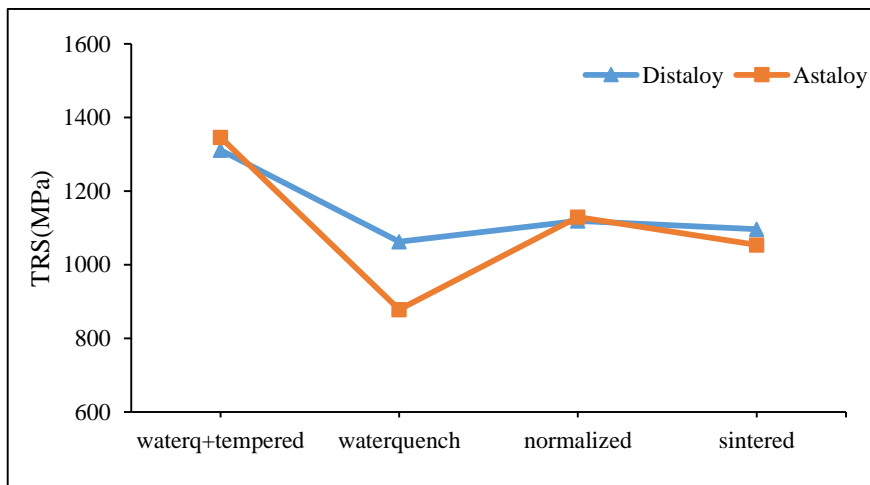


Figure 4.37 Comparison of TRS values for Distaloy and Astaloy with various heat treatments.

CHAPTER 5

DISCUSSION

In this study, Distaloy DH and Astaloy Mo powder alloys are used in order to study the formation of upper bainite and lower bainite by isothermal treatments at 300°C and 450°C. For comparison purposes, the microstructure and mechanical properties of sintered, normalized and quenched samples are also utilized.

To obtain upper and lower bainite morphologies, the isothermal heat treatments are done by quenching the specimens into a salt bath. The M_s and B_s temperature of the alloys are calculated using the equations 4.1 and 4.2. These temperatures are important since the quenching temperature dictates whether a lower or upper bainite will form.

5.1 The Porosity Content of Distaloy DH and Astaloy Mo

Both Distaloy DH and Astaloy Mo have the same chemical composition, as shown in Table 3.1. Both of them are prealloyed powders, but in Astaloy Mo, copper is added by admixing method. The effect of copper addition method on the porosity content of sintered samples is given in Table 4.2. Astaloy Mo sintered samples have a slightly higher percentage of porosity than Distaloy DH. Moreover, as shown in Figure 4.3 in Astaloy Mo, the pore size and distribution of them are heterogeneous. It seems that the admixing method for copper content does not yield a homogeneous distribution of copper in the composition. In Distaloy DH samples, the Cu is diffusion bonded. The positive effect of copper on sintered densities is well documented [9, 13, 16, 17, 23, 27]. Copper is liquid at sintering temperature

(1120°C) and most probably spreads through the powder particles during sintering. A more homogeneous distribution of the Cu in the matrix, as in the case of Distaloy-DH seems to effect the densification more positive with less amount of porosity.

5.2 Microstructural Development of Heat Treated Specimens

In this study, the specimens are sintered at 1120°C as an initial step. After sintering, several specimens are heat treated to obtain different type of microstructures. The M_s and B_s temperatures are calculated as 235°C and 516°C using the equations 4.1 and 4.2 .Therefore, an isothermal treatment just below B_s could yield an upper bainitic structure. On the other hand, an isothermal treatment just below M_s could yield a lower bainitic structure. Therefore, the mechanical behavior of upper and lower bainitic microstructures could be investigated in detail.

By selecting the isothermal treatment time carefully, it is aimed to obtain a mixture of bainite + martensite phases. After an isothermal treatment for 5 minutes at 300°C, the transformation is completed only 50% and yielded 50% martensite – 50% lower bainite. Increasing the transformation time to 15 minutes, yielded 25% Martensite and 75% lower bainite. The behavior of the matrix consisting of bainite (tough phase) and martensite (hard but brittle phase). Hence, a reduction in macrohardness values was observed with an increase in isothermal holding time due to the decrease in martensite content.

On the other hand, isothermal heat treatment at 450°C lead to upper bainitic microstructure in both Distaloy DH and Astaloy Mo samples. In comparison to lower bainitic microstructures, there is not a major difference between the macrohardness values of samples with different isothermal holding times.

For comparison purposes, several sintered specimens are quenched to obtain 100% martensitic structure. Normalizing (cooling in air) is also applied to see the microstructural development.

For isothermally heat treated samples at 450°C for both Distaloy DH and Astaloy Mo samples, upper bainite phase mixture is observed. Depending on the region, both fine and coarse lamellar morphology of upper bainite are seen in the same sample.

An isothermal treatment at 300°C caused formation of lower bainite phase in both Astaloy Mo and Distaloy specimens. The morphology of lower bainite is in the form of sheaves of bainite with lath-like ferrites. The spacing between the sheaves are very fine. Due to this morphology, lower bainite yields higher strength values in comparison to upper bainitic microstructures.

At definite regions of the specimens treated at 300°C, several transformation products are also observed with different morphologies. At higher magnifications, some of these regions were found to be lower bainite but having much finer sheaves. Several others could not be identified.

As far as the sintered and normalized samples are concerned, pearlite phase is also observed. However, the morphology of the pearlite is different. At definite regions, the cementite has an acicular structure. This is attributed to the presence of Mo in the steel, which probably modifies the pearlitic structure. Based on Lindsley and Rutz' study, adding molybdenum to powder alloys the ferrite-carbide microstructure in a way that the lamellar structure vanishes and instead acicular ferrite with carbide and/or upper bainite emerges [24]. Furthermore, as demonstrated in Mazancova et al., the formation of bainite takes place with similar transformation mechanisms in the same temperature range with acicular ferrite [30]. The production of degenerated pearlite structure with acicular ferrite and carbide appears to be improved in the presence of molybdenum.

5.3 Mechanical Characterization of Heat Treated Samples

Figure 4.31, Figure 4.32 and Table 4.6 show the hardness values of different heat treated, Distaloy DH and Astaloy Mo samples. As expected, water quenched samples of both compositions have highest hardness values among all other

treatments 396 HB for Distaloy and 410 HB for Astaloy. When quenched samples tempered, the hardness is decreased to 359 HB for Distaloy DH and 387 HB for Astaloy Mo as expected. These hardness values are low when compared to conventional steels. However, the presence of pores in sintered specimens is believed to be responsible from these low hardness values.

Macrohardness values of as-sintered and normalized samples are very low, i.e. 187 HB and 196 HB for Distaloy and 184 HB and 221 HB for Astaloy respectively. The presence of pearlite phase seems to cause low hardness values in these specimens.

When the isothermal treated specimens are concerned, the specimens treated at 450°C yield very similar hardness values to that of normalized specimens. The hardness of specimens treated at 450°C is in the range 186 HB-177 HB for Distaloy DH, whereas a normalizing treatment yields 196 HB. The equal or even higher hardness of the normalized specimen can be explained with the presence of a few amount of martensite (Figure 4.5). A similar trend is also observed in Astaloy Mo. The specimens treated at 450°C have hardness values in the range of 175-250HB and normalized sample hardness value is 221 HB.

The specimens treated at 300°C yields hardness values in the range 300HB-260HB, which are considerably higher than both normalized and 450°C treated samples. As expected, the hardness values of the lower bainitic steels are lower than quenched and tempered specimens.

Another important fact for the specimens treated at 300°C is the decrease in their hardness values with an increase in holding time. For example, in Distaloy DH, the hardness of the specimen hold only 5 minutes at 300°C yields a hardness value of 302HB. When the holding time at 300°C is increased to 15 minutes and 30 minutes, the hardness values decrease from 290HB and 260HB respectively. A similar drop in hardness values are also observed for Astaloy Mo specimens: hardness values decrease from 275HB to 175HB in Astaloy Mo Samples as well. The change in the

hardness values can be explained with the amount of martensite. As shown previously in percentage of martensite Table 4.3 and Table 4.4 amount of martensite decreases with an increase in isothermal heat treatment period from 5 minutes to 15 minutes for both Astaloy and Distaloy.

As far as the TRS values are concerned, there is a correlation between the hardnesses and TRS values of the specimens. The specimens with higher hardness values also yield high TRS values. For example, the specimens treated at 300°C have TRS values in the range 1250-1400 MPa, whereas the specimens treated at 450°C have TRS values only 1080-1140 MPa.

Transverse rupture strength values of upper bainitic microstructures are lower than quenched and tempered martensitic microstructures and comparable to normalized samples. In this regard, isothermal treatment at 450°C which lead to completely upper bainitic microstructures does not give higher strength values in comparison to normalized samples.

There is no substantial difference between the TRS values of as-sintered and normalized samples, which are in the range of specimens treated at 450°C. However, the comparison of TRS values of the specimens treated at 300°C with that of quenched, quenched and tempered specimens yield interesting results. The as-quenched sample yields lower TRS values (1000 MPa) with respect to quenched and tempered specimens (1300 MPa) and specimens' treated at 300°C (1350 MPa). This reduction can be attributed to the brittle nature of the martensite in as-quenched condition. In addition, several other studies show that while untempered martensite is present in the microstructure, the strength of the specimens decreases [47,48].

More importantly, the specimens having lower bainite in their microstructure (i.e. 300°C samples) yields identical or higher TRS values with respect to quenched and tempered specimens. The TRS values of martensitic specimen is in the range 1310 MPa, whereas the TRS value of 100% lower bainitic specimen is 1327 MPa for

Distaloy DH. A similar trend is also observed for Astaloy Mo specimens such that the TRS values of martensitic and lower bainitic specimens are 1345 MPa and 1290 MPa respectively (which are very close within the error limits).

As far as the TRS values are concerned, it can be concluded that hardness values of the specimens are not the only parameter that determines the TRS values. Generally, the higher the hardness values the higher the TRS values. However, lower bainitic specimens can yield comparable or even high TRS values at low hardness levels in comparison to martensitic specimens. Therefore, the microstructure can be an important factor in defining the bending strength values.

Isothermal heat treatment at 300°C, always lead to higher TRS values in Distaloy DH samples in comparison to Astaloy Mo samples, although both have similar microstructures (martensite+lower bainite or lower bainite). This might be correlated to the higher densities attained in Distaloy DH after sintering. However, further work is required here in order to elucidate this point.

CHAPTER 6

CONCLUSIONS

In this study, the effect of Mo, Cu and C and different heat treatments on the development of the microstructure is investigated. In addition, the relation between the microstructure and mechanical properties of the specimens are examined. The alloys were sintered at 1120°C for 45 minutes in laboratory scale furnace and then different heat treatment are applied on samples. The following conclusions are reached:

- 1) The porosity percentage of Distaloy DH samples are lower than Astaloy Mo samples due to the better distribution of copper in diffusion bonded powder.
- 2) Isothermal heat treatment at 300°C revealed a mixture of lower bainite and martensite microstructure. Increasing the isothermal holding time from 5 minutes to 30 minutes lead to completely lower bainitic microstructures. Hence, a reduction in macrohardness values was observed with an increase in isothermal holding time due to the decrease in martensite content.
- 3) Isothermal heat treatment at 450°C lead to upper bainitic microstructure in both Distaloy DH and Astaloy Mo samples. In comparison to lower bainitic microstructures, there is not a major difference between the macrohardness values of samples with different isothermal holding times.
- 4) Isothermal heat treatment at 300°C for 15 minutes lead to the highest TRS values among all the samples. The fully lower bainitic microstructure

obtained after this treatment yields 10% higher TRS values in comparison to quenched and tempered martensitic microstructures.

- 5) Transverse rupture strength values of upper bainitic microstructures are lower than quenched and tempered martensitic microstructures and comparable to normalized samples. In this regard, isothermal treatment at 450°C which lead to completely upper bainitic microstructures does not give higher strength values in comparison to normalized samples.
- 6) Isothermal heat treatment at 300°C, always lead to higher TRS values in Distaloy DH samples in comparison to Astaloy Mo samples, although both have similar microstructures (martensite+lower bainite or lower bainite). This might be correlated to the higher densities attained in Distaloy DH after sintering. However, further work is required here in order to elucidate this point.

REFERENCES

- [1] Narasimhan, K.S, "Sintering of powder mixtures and the growth of ferrous powder metallurgy," *Materials Chemistry and Physics*, p. 56–65, 2001.

- [2] Bocchini G. F., Rivolta B., Silva G., Poggio E., Pinasco M. R., Ienco M.G, "Microstructural and Mechanical Characterisation of Some Sinter Hardening Alloys and Comparisons with Heat Treated PM Steels," *Powder Metallurgy*, pp. 343-351, 2004.

- [3] James, W.B, "What is Sinter Hardening?," in *International Conference on Powder Metallurgy & Particulate Materials*, Las Vegas, Nevada USA., 1998.

- [4] Bhadeshia, H.K, *Bainite in Steels Transformations, Microstructure and Properties*, Cambridge, 2nd Edition ed. 2001.

- [5] Singh U.P, Roy.B, Bhattacharyya.S.K, "Microstructure and mechanical Properties of as-rolled high strength bainitic rail steels IOM Communications limited London 2001," *Material Sciences and Technology*, vol. 17, pp. 34-38, 2001.

- [6] Lan, H, Du, L.X, Misra, R.D.K, "Effect of microstructural constituents on strength–toughness combination in a low carbon bainitic steel," *materials science and engineering*, pp. 194-200, 2014.

- [7] Kapito, A.; Stumpf, W; Papo, M.J, "The role of alloying elements in bainitic rail steels," *Southern African Institute of Mining and Metallurgy*, vol. 113, pp. 67-72, 2013.
- [8] Bhadeshia, H.K, "Improvements in and relating to carbide-free bainitic steels and methods of producing such steels," *International Patent application WO 96/22396, published under the Patent Cooperation treaty (PCT)*..
- [9] Singh, R, "Introduction to Basic Manufacturing Process and Workshop Technology," *New Age International*, 2006.
- [10] German R.M, *Powder Metallurgy of Iron and Steel*, University Park, Pennsylvania: the Pennsylvania State University, 1998.
- [11] Abdoos H., Khorsand H., Shahani A. R., "Fatigue behavior of diffusion bonded powder metallurgy steel with heterogeneous microstructure," *Materials and Design*, pp. 1026-1031, 2009.
- [12] James W. B., OtBrien R.C., "High Performance Ferrous P/M Materials: The Effect of Alloying Method on Dynamic Properties," *Metal Powder Report*, 1987.
- [13] Höganäs Handbook for Sintered Components:, " Sintered Iron Based Materials,," in *PM School Handbook*, 2004.
- [14] Murphy T. F., Baran M.C, "An Investigation into the Effect of Copper and Graphite Additions to Sinter-Hardening Steels," in *PM² TEC 2004*

International Conference on Powder Metallurgy & Particulate Materials, 2004.

- [15] Engström U., Lindberg C, Tengzelius J, "Powders and processes for high performance PM steels," *Powder Metallurgy*, pp. 67-72, 1992.
- [16] Vara Prasada Rao, K, *Manufacturing Science & Technology- Manufacturing Processes and Machine Tools*, Principal, Loyola Institute of Tech. & Mgmt., Guntur, Andhra Pradesh: New Age International, 2002.
- [17] German, R.M, *Liquid Phase Sintering*, Springer Science & Business Media, 1985.
- [18] Asm International Handbook Committee, *ASM Handbook: Powder Metal Technologies and Applications*, vol7, ASM International, 1998.
- [19] Hatami, S., Malakizadi, A., Nyborg, L., Wallin, D, "Critical aspects of sinter-hardening of prealloyed Cr-Mo steel," *Materials Processing Technology*, vol. 210, pp. 1180-1189, 2010.
- [20] German, R, "Powder Metallurgy Science," Princeton, Metal Powder Industries Federation, 1994, pp. 380-390.
- [21] Ridal K.A. and McCann J, "Physical Properties of Martensite and bainite," Iron and Steel Institute, london, 1965.
- [22] James, B, "Recent Developments in Ferrous Powder Metallurgy Alloys," *Powder Metallurgy*, 1994.

- [23] Lenel V, Fritz, Powder Metallurgy- Principles and Applications, Princeton, New Jersey: Metal Powder Industries Federation, 1980.
- [24] Totten G. E, Steel Heat Treatment Metallurgy and Technologies, CRC Press, Taylor & Francis Group, 2007.
- [25] Murphy, B, "Dimensional Control in Cu-Ni containing Ferrous," Cinnaminson, NJ, Hoeganaes Corporation.
- [26] Chuang, K.H., "Improved distribution of nickel and carbon in sintered steels through addition of chromium and molybdenum," *Powder Metallurgy*, vol. 51, 2008.
- [27] Larsson, M, "Mechanical properties and dimensional stability obtained with different alloying techniques," Höganäs, Sweden : Höganäs AB.
- [28] Porter, D.A, Easterling, K.E, "Phase transformations in Metals and Alloys," T.J. Press, Cornwall, 1992.
- [29] Wu .M. W., K. S. Hwang., H. S. Huang , "Improved distribution of nickel and carbon in sintered steels through addition of chromium and molybdenum," *Powder Metallurgy*, vol. 51, 2008.
- [30] ASM Handbook, Properties and Selection: Irons, Steels, and High-Performance Alloys, ASM international, Vol 1, 1998.
- [31] Lawley, A, "Microstructure and Mechanical properties of a bainitic pm steel," Hoeganaes Corporation Cinnaminson.

- [32] Höganäs Handbook for Sintered Components, Sintered Iron Based Materials, PM School Handbook, 2015.
- [33] Rutz H. G., Graham A.H, "Sinter-Hardening P/M Steels," in *P/M Steels. in PM²TEC '97 International Conference on Powder Metallurgy & Particulate Materials*, Chicago, USA, 1997.
- [34] Rees G.I., Bhadeshia H.K, " Part I, Modified Model," in "*Bainite Transformation Kinetics*, 1992, pp. 985-993.
- [35] Causron R.J., Fulmer J.J., Sinter Hardening Low-Alloy Steels, "Sinter Hardening Low-Alloy Steels," in *PM² TEC 2002 International Conference on Powder Metallurgy & Particulate Materials*, San Francisco, 1992.
- [36] Lindsley B., Rutz H, " Effect of Molybdenum Content in PM Steels," *Advances in Powder Metallurgy & Particulate Materials*, 2008.
- [37] Marucci M. L., Baran.M.C, Narasimhan K.S, "Properties of High Density Sinter-Hardening P/M Steels Processed Using an Advanced Binder System," in *PM²TEC2002 World Congress on Powder Metallurgy & Particulate Material*, Orlando, 2002.
- [38] Baran, M, "Application of Sinter-Hardenable Materials for Advanced Automotive Applications such as Gears, Cams, and Sprockets," in *International Powder Metallurgy Congress*, Munich, German, 2000.

- [39] Berg, S, "P/M Steel Suitable for Sinterhardening in Respect of Cost and Performance," in *PM² TEC 2001 International Conference on Powder Metallurgy & Particulate Materials*, New Orleans, USA, 2001.
- [40] Maroli B., Berg S., Lewenhagen J, "Properties and Microstructure of PM Materials Pre-alloyed with Nickel, Molybdenum and Chromium," in *EURO PM'*, 2001.
- [41] Youseffi M., Wright C.S., Jeyacheya F. M, "Effect of carbon content, sintering temperature, density, and cooling rate upon properties of prealloyed Fe -1.5Mo powder," *Powder Metallurgy*, pp. 270-274, 2000.
- [42] Totten.G.E, *Steel Heat Treatment Handbook*, Oregon, U.S.A, 2006.
- [43] Engström U., McLelland J., Maroli B , "Effect of Sinter Hardening on the Properties of High Temperature Sintered PM Materials," in *PM²TEC 2002 International Conference on Powder Metallurgy & Particulate Materials*, 2002.
- [44] Chagnon F., T.Y., "Effect of Copper Additions on Properties of 1.5% Mo Sintered Steels," in *PM² TEC 2002 International Conference on Powder Metallurgy & Particulate Materials*, Orlando, 2002.
- [45]] Wong-Ángel, W.D., Téllez-Jurado, L., Chávez-Alcalá, J.F., Chavira-Martínez, E., Verduzco-Cedeño, V.F, "Effect of Copper on the Mechanical Properties of Alloys Formed By Powder Metallurgy," *Materials & Design*, pp. 12-18, 2014.

- [46] Mazancova, E., Jonsta, Z., Wyslych, P., Mazanec, K, "Acicular Ferrite and Bainite Microstructure and Properties and Comparison of Their Physical Metallurgy Response," in *14. International Metallurgy & Material Conference*, 2005.
- [47] Straffelini G., Fontanari V., Hafez A., Molinari A, "Comparison of Impact and Slow Bend Behavior of PM Ferrous Alloys," *Materials Science and Engineering*, vol. 52, pp. 153-160, 1998.
- [48] Straffelini G., Menapace C., Molinari A, "Interpretation of Effect of Matrix Hardening on Tensile and Impact Strength of Sintered Steels," *Powder Metallurgy*, vol. 45, pp. 167-172, 2002.